Molybdenum disulfide and molecular thin films integration into devices for molecular electronics and spintronics

Master thesis

TECHNICKÁ UNIVERZITA V LIBERCI
Fakulta mechatroniky, informatiky a mezioborových studií

Integrace sulfidu molybdeničitého a molekulárních tenkých vrstev v zařízeních pro molekulární elektroniku a spintroniku

Diplomová práce

Liberec 2019

Technická univerzita v Liberci
Fakulta mechatroniky, informatiky a mezioborových studií
Akademický rok: 2018/2019

ZADÁNÍ DIPLOMOVÉ PRÁCE
(PROJEKTU, UMĚLECKÉHO DÍLA, UMĚLECKÉHO VÝKONU)

Jméno a příjmení: **Bc. Josef Světlík**

Osobní číslo: **M16000165**

Studijní program: **N3942 Nanotechnologie**

Studijní obor: **Nanomateriály**

Název tématu: **Integrace sulfidu molybdeničitého a molekulárních tenkých vrstev v zařízeních pro molekulární elektroniku a spintroniku**

Zadávající katedra: **Katedra chemie**

Zásady pro vypracování:

1. Integration of MoS_2 into horizontal devices.

2. New MoS_2-based vertical device fabrication process development.

3. Testing of vertical devices fabricated by UHV evaporation.

Rozsah grafických prací: **dle potřeby**

Rozsah pracovní zprávy: **40-50 stran**

Forma zpracování diplomové práce: **tištěná**

Jazyk zpracování diplomové práce: **Angličtina**

Seznam odborné literatury:

1. Q. H. Wang, Nat. Nanotechnol., 7, 683, 2012.

2. S. Z. Butler et al., ACS Nano, 7, 4, 2898, 2013.

3. C. Felser et al. Angew. Chemie, 46, 668-699, 2007.

4. M. Piquemal-Banci, J. Phys. D. Appl. Phys., 50, 203002, 16, 2017.

5. H. Li et al., ACS Nano, 7, 11, 10344-10353, 2013.

6. H. Li et al., Adv. Funct. Mater., 22, 1385-1390, 2012.

Vedoucí diplomové práce: **RNDr. Michal Řezanka, Ph.D.**
Katedra chemie

Konzultant diplomové práce: **Marta Galbiati, Ph.D.**
University of Valencia

Datum zadání diplomové práce: **10. října 2018**

Termín odevzdání diplomové práce: **30. dubna 2019**

prof. Ing. Zdeněk Plíva, Ph.D.
děkan

L.S.

prof. Ing. Josef Šedlbauer, Ph.D.
vedoucí katedry

V Liberci dne 10. října 2018

Prohlášení

Byl jsem seznámen s tím, že na mou diplomovou práci se plně vztahuje zákon č. 121/2000 Sb., o právu autorském, zejména § 60 – školní dílo.

Beru na vědomí, že Technická univerzita v Liberci (TUL) nezasahuje do mých autorských práv užitím mé diplomové práce pro vnitřní potřebu TUL.

Užiji-li diplomovou práci nebo poskytnu-li licenci k jejímu využití, jsem si vědom povinnosti informovat o této skutečnosti TUL; v tomto případě má TUL právo ode mne požadovat úhradu nákladů, které vynaložila na vytvoření díla, až do jejich skutečné výše.

Diplomovou práci jsem vypracoval samostatně s použitím uvedené literatury a na základě konzultací s vedoucím mé diplomové práce a konzultantem.

Současně čestně prohlašuji, že texty tištěné verze práce a elektronické verze práce vložené do IS STAG se shodují.

25. 4. 2019   Bc. Josef Světlík

Acknowledgement

Abstract

Classical devices employing Si are almost reaching their physical limits and alternatives, based on entirely new materials and principles, are being investigated and slowly penetrate from laboratory to industry. Examples of such new materials, which appear promising to be once used in the semiconducting industry, are two-dimensional (2D) materials and functional molecules due to their small dimensionality, low price, and unique functionalities.

This master thesis focuses on techniques to integrate 2D materials and molecular thin films into devices and study their properties. First, a molybdenum disulfide (MoS_2)-based field-effect transistor (FET) was fabricated and functionalized with spin-crossover (SCO) nanoparticles (NPs). Effect of SCO NPs on MoS_2 electronic properties by switching between two distinct states using an external stimulus was investigated. Second, an integration method of 2D materials into a magnetic tunnel junction (MTJ) was being developed for spintronic applications. Benefits and drawbacks of the chosen method are discussed. Finally, the possibility to integrate thin SCO molecular films into vertical spin-valves directly through their evaporation using a shadow mask was investigated.

Keywords: 2D materials, molybdenum disulfide, spin-crossover molecules, spin-crossover nanoparticles, electronics, spintronics.

Abstrakt

Klasické zařízení, využívající Si, téměř dosahují svých fyzikálních limit a alternativy založené na zcela nových materiálech a principech jsou zkoumány a pomalu přecházejí z laboratoří do průmyslu. Příkladem těchto nových materiálů, které se zdají býti slibné pro jejich budoucí využití v polovodičovém průmyslu, jsou dvou-dimenzionální (2D) materiály a funkční molekuly díky jejich malým rozměrům, levnosti a nevšedním vlastnostem.

Tato diplomová práce se zaměřuje na integrační techniky 2D materiálů a molekulárních tenkých vrstev do zařízení a na studium jejich vlastností. Nejdříve je využit sulfid molybdeničitý (MoS_2) k přípravě tranzistoru a následně funkcionalizován spin-crossover (SCO) nanočásticemi (NPs). Vliv SCO NPs na elektronické vlastnosti MoS_2 skrze spínání mezi dvěma odlišnými stavy s využitím vnějšího stimulu je zkoumán. Dále je vyvíjena integrační metoda 2D materiálů do magnetického tunelovacího spoje (MTJ) pro spintronické aplikace. Výhody a nevýhody zvolené metody jsou diskutovány. Nakonce je vyšetřována možnost integrace tenkých molekulárních vrstev do vertikálních zařízení přímo skrze jejich napařování s pomocí stínící masky.

Klíčová slova: 2D materiály, sulfid molybdeničitý, spin-crossover molekuly, spin-crossover nanočástice, elektronika, spintronika.

Table of Contents

Abbreviations

2D	two-dimensional
AFM	atomic force microscope
e-beam	electron-beam
FET	field-effect transistor
FM	ferromagnetic
HS	high spin
ICMOL	Institute of Molecular Science
LS	low spin
MBE	molecular beam epitaxy
MoS_2	molybdenum disulfide
MR	magnetoresistance
MTJ	magnetic tunnelling junction
NPs	nanoparticles
OLEDs	organic light emitting diodes
OM	optical microscopy
P	pairing energy
PC	polycarbonate
PDMS	poly(dimethylsiloxane)
phen	1,10-phenanthroline
PMMA	poly(methyl methacrylate)
PPMS	physical property measurement system
pz	pyrazolyl
RMS	root mean squared

SCO	spin-crossover
TMDCs	transition metal dichalcogenides
trz	1,2,4-triazole
UHV	ultra-high vacuum
vdW	van der Waals
Δ	ligand field splitting

Motivation and Goals of This Work

In 1965 Dr Gordon E. Moore, later co-founder of N M Electronics (todays Intel Corporation), published an article[1] where he predicts a bright future for the electronic industry. His observation of shrinking size of transistors resulted in prediction which empirically proved to be correct and turned into a notional law. The Moore's law says that transistor count (the number of transistors on a dense integrated circuit) doubles approximately every two years which results in doubled performance of a device. Graph in semilogarithmic scale of exponential growth of transistor count can be seen in the **Figure 1**. In the upcoming years, Moore's law changed from being a measure of progress to a driving force.
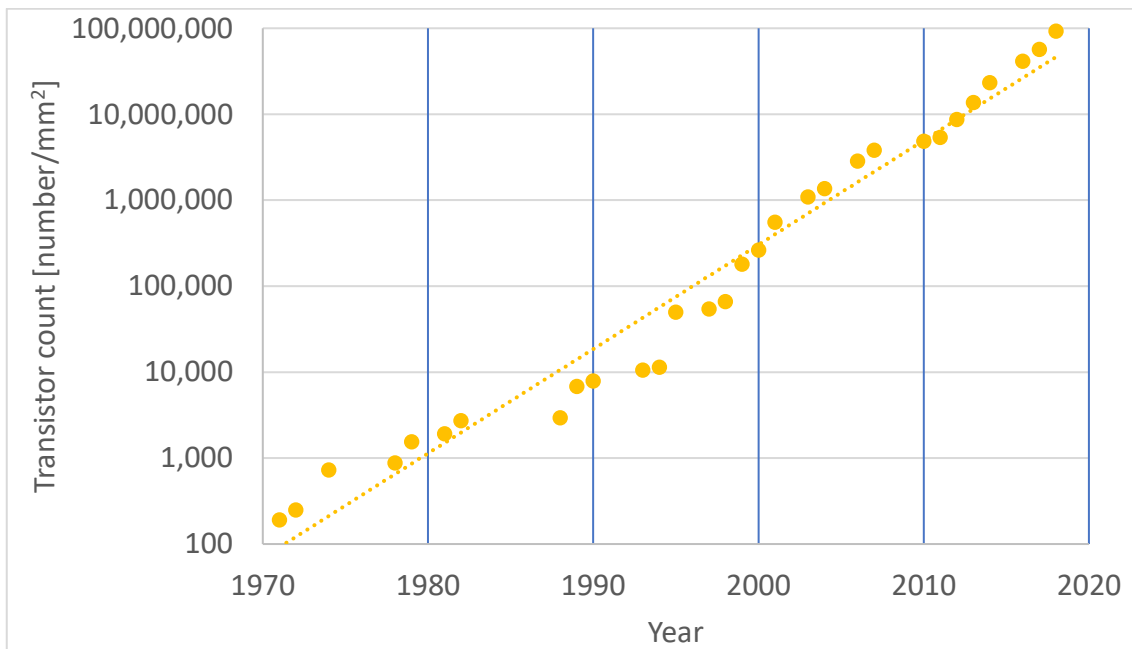
Figure 1: Graphical representation of Moore's law (1971-2018); dotted line represents an extrapolation curve of presented data.

Although researchers and engineers were able to follow the pace of advances in electronics predicted by Dr Moore for about 50 years[2] shifting the technological limits ever further, intrinsic physical limitations of Si/SiO_2-based transistors will be an issue soon and it will make further downscaling impossible[3].

To overcome this obstacle, current material research not only aims at finding materials which would possess better characteristics than those of Si and SiO_2 but especially at finding materials with new functionalities. Employment of these materials in electronics

through the fabrication of devices with novel architectures could be an alternative road to the Si-based semiconducting industry and could offer an extension of Moore's law leading to further growth of computing power, storage density and decrease in energy consumption.

Among all possible candidates, 2D materials, together with functional molecules seem to be a good choice between these new materials, partially thanks to their high versatility. In both cases, materials display a full range of electrical, optical and magnetic properties, and therefore could find many distinct applications in a new generation of devices.

Moreover, it appears to be advantageous to combine them, both, different 2D materials together[4], and 2D materials with functional molecules[5], in heterostructures, which gives rise to unusual physical phenomena. The fabrication of hybrid organic/inorganic devices is of great potential thanks to the versatility of molecules and the possibility to synthesise desirable molecules with predictable functionalities, giving additional degrees of freedom to devices[6].

Institute of molecular science (ICMOL), where I conducted my research, has a strong expertise in a growth and characterisation of 2D materials, synthesis of SCO molecules and SCO NPs and recently is focusing on the integration of these materials into devices for spintronic and electronic applications. A closer cooperation between physicists and chemists at this institute allows all the steps from material conception to its integration and measurement in devices to be performed in the same laboratory.

Thanks to this close collaboration, in this work, we aim at developing procedures for the fabrication of 3 kinds of devices:

1. First, we intend to fabricate MoS_2-based transistors functionalized with SCO NPs to measure the possible effect of SCO NPs on electrical properties of MoS_2 due to their spin-crossover, realised by temperature change. MoS_2 was chosen as a prototypical 2D material showing strain-induced change of band structure. Moreover, it is air-stable, thus in contrast to many other 2D materials, glove-box manipulation is not needed, and more straightforward work on air can be performed.

2. Also, we investigated the possibility to integrate MoS_2 into magnetic tunnel junction for spintronics. Since the main current technological issue of 2D material-based vertical devices fabrication is oxidation of ferromagnetic (FM)

electrodes, our goal is to develop an integration method based on the use of Si_3N_4 membranes to avoid exposure of oxidation-sensitive parts of the device to the air. Again, we have chosen MoS_2 since it is representative and well characterised 2D material. Apart from that, it was predicted that MoS_2 could bring interesting features to magnetic tunnel junction, such as high magnetoresistance values up to 300 %[7,8].

3. Finally, we aim to integrate sublimable SCO molecules into vertical spin-valves. To do that, we use a set of shadow masks to evaporate ferromagnetic electrodes in a cross-junction geometry inside a UHV chamber. SCO molecules are evaporated in the form of thin layers over the substrate with previously evaporated bottom electrodes. The goal of this project is to test if the SCO molecules are suitable to be used as a spacer layer and if they could give additional functionality to vertical spintronic devices. Nevertheless, the first objective is to optimize the fabrication method itself since it was new in ICMOL's laboratory. In this scenario, we aim to find the minimal thickness of the SCO molecular layer, for which pinhole-free devices still can be obtained. Moreover, we target to test the use of a carbon layer as a barrier to limit pinholes formation.

1 Theoretical Part

The research field of two-dimensional (2D) materials has appeared relatively recently in 2004 when A. Geim and K. Novoselov isolated and characterized graphene for the first time[9]. Graphene is a single layer of graphite that was obtained from its exfoliation using scotch tape. Since this novel material has many appealing mechanical, chemical, optical and electrical properties (such as high Young's modulus and selective reactivity of edges, high opacity and electron mobility)[10,11], it has captured a lot of scientific attention which has brought many interesting applications (e.g. solar cells, flexible displays, supercapacitors, etc.)[12]. However, there is one main limitation for the use of graphene resulting from its electronic gapless Dirac cone band structure: graphene does not show semiconducting behaviour, and, for example, it is not suitable to be used in transistors or optoelectronic devices. This obstacle generated a search for alternative materials.

Graphite indeed is not the only layered crystal, and many other mono-atomically thick materials with different chemical nature were prepared and intensively investigated during the last years[13]. It was found that 2D materials present a full range of electrical and magnetic properties: from superconductors to insulators and from ferromagnetics to diamagnetics[14]. Thus, one has a full pallet of materials with distinct properties from which it is possible to build a nanodevice or combine their properties in heterostructures[4]. Moreover, a new research direction is the possibility to add new functionalities to these materials, for example with their functionalization with functional molecules that change their properties with an external stimulus (temperature, light, etc.)[6].

This tunability of 2D materials and versatility of functional molecules plus their inherent small dimensionality make them an interesting building block for their application in molecular electronic and spintronic devices, towards the research for alternatives to present Si-based electronics.

Besides graphene, MoS_2 has become a prototypical 2D material thanks to its intriguing properties, such as mechanical flexibility, air stability, and semiconducting behaviour with tunable bandgap.

1.1 Molybdenum Disulfide

Silvery black inorganic compound molybdenum disulfide (MoS_2) is abundantly present in nature as mineral molybdenite. It belongs to the group of transition metal dichalcogenides (TMDCs), which consist of a transition metal (M = Ti, Zr, Hf, V, Nb, Ta, Mo, W, Tc, Re, Co, Rh, Ir, Ni, Pd, Pt) and two chalcogen atoms (X = S, Se, Te) and possess generalized formula MX_2. TMDCs have representatives of (semi)metallic, semiconducting and even superconducting behaviour depending on their crystal structure and chemical composition[15].

Many representatives of TMDCs family have layered structure including MoS_2. Individual layers consist of covalently bonded molybdenum cations to sulphur anions (S^{2-}-Mo^{4+}-S^{2-}), with bond-length of around 2.4 Å where Mo ions stay in their own planes sandwiched by two sulphide planes (**Figure 2a**). These compact tri-atomic layers are stacked together with layers of the same kind and held together by relatively weak van der Waals (vdW) interactions in distance of approximately 6.5 Å. VdW forces can be easily overcome, and crystal is exfoliated in thin layers, down to the monolayer.
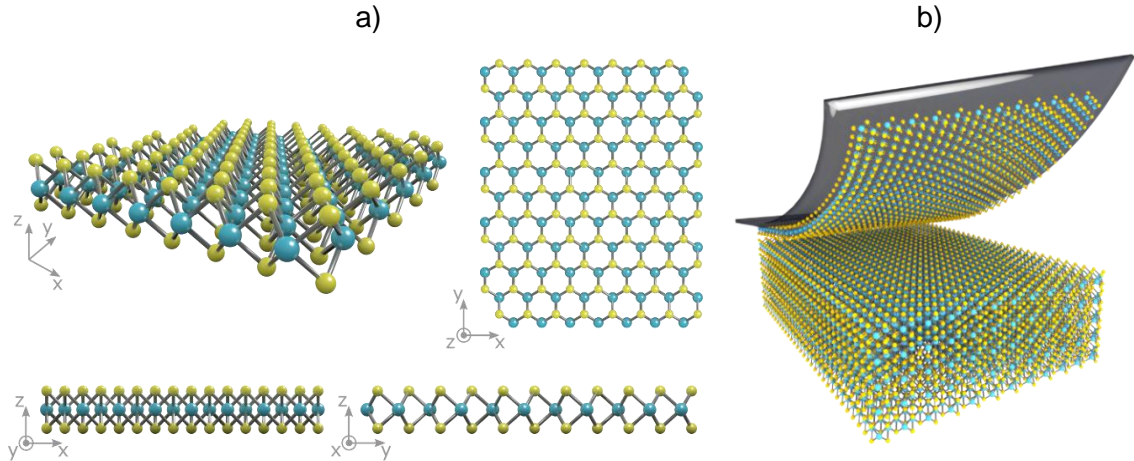
*Figure 2: Crystal structure of MoS₂: **a)** Monolayer composed of Mo (blue) and two S (yellow) planes held together by covalent bonds; **b)** Mechanical exfoliation from bulk crystal. Figure reproduced with permission from ref. 16, © 2019 Ossila.*

Mechanical exfoliation is one possible way how to do that. This technique applies a mechanical force to separate layers of bulk 2D material. It uses a scotch tape where glue works as an adhesive material for the separation of part of the crystal (**Figure 2b**). The advantage of this method is its simplicity, rapidity and possibility to obtain high-quality flakes with size typically from few to tens of micrometres. This makes it the most suitable technique to get high quality 2D layers for laboratory studies. Nevertheless, drawbacks

of this technique are possible surface contamination of 2D materials by polymeric particles of glue, low yield, low control over size and number of layers.

Hexagonal MoS_2 is semiconducting material and as its number of layers varies, band gap of the material changes from indirect 1.2 eV in bulk to large direct 1.87 eV in monolayer limit (**Figure 3**)[17].
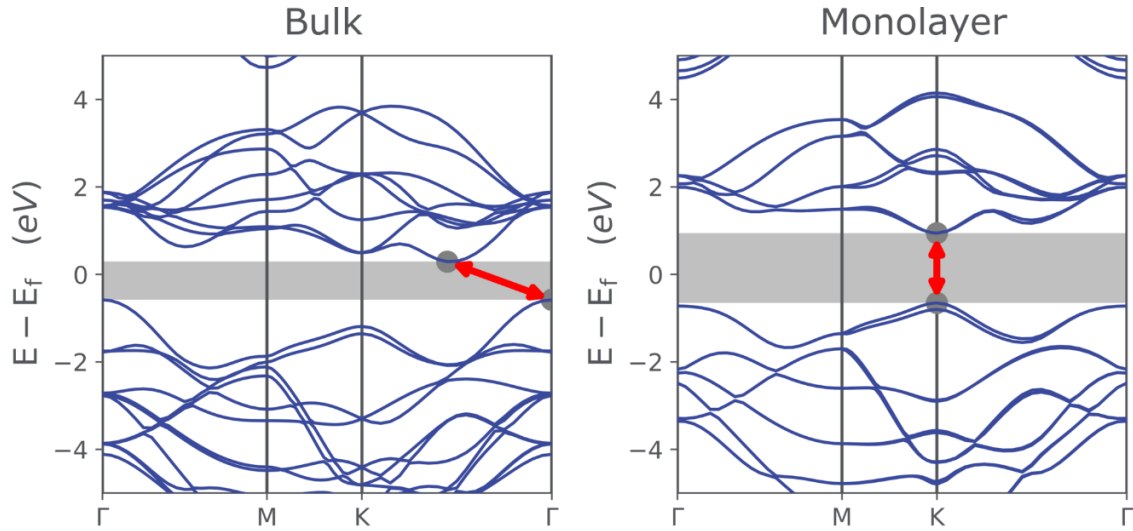

Figure 3: Electronic structure of bulk and monolayer MoS_2. Figure reproduced with permission from ref. 16, © 2019 Ossila.

Since MoS_2 possesses many appealing physical, optical and electrical properties[18], such as high mechanical strength[19], piezoelectricity[20], direct bandgap in monolayer mode[21], and decent mobility of approximately 350 $cm^2.V^{-1}.s^{-1}$, it has been studied for a wide variety of applications, such as field-effect transistors (FETs)[22], resonators[23], amplifiers[24], sensors[25], spintronic devices[8], photodetectors[26], photovoltaic devices[27], electrocatalysis for hydrogen evolution reaction[28] and lithium-ion batteries[29]. Apart from that, MoS_2 has been used as a lubricant for a long time, due to its low coefficient of friction.

Another property that has recently attracted an increasing interest is the strain effect on MoS_2. Indeed, it was theoretically predicted by first principle calculations that strain on 2D MoS_2 could change its electronic structure. Namely direct to indirect and semiconductor to metal transition under elastic strain have been predicted[30].

According to previous theoretical studies, exact change of electronic structure depends on the form of strain. Out of plane uniaxial compression applied on monolayer MoS_2 results in gradual cross-over from semiconducting to metallic state (**Figure 4a**), while hydrostatic compression cause increase of bandgap (**Figure 4b**)[31]. Different response of the material can be also seen for biaxial tensile and biaxial compressive in-plane strain. Biaxial tensile strain causes steeper shrinking of bandgap, while during compressive strain small increase of bandgap for low stress can be observed before subsequent decreasing of bandgap occurs (**Figure 4c**). In both cases, even application of small strain (around 2 %) already results in direct-indirect bandgap transition[32].
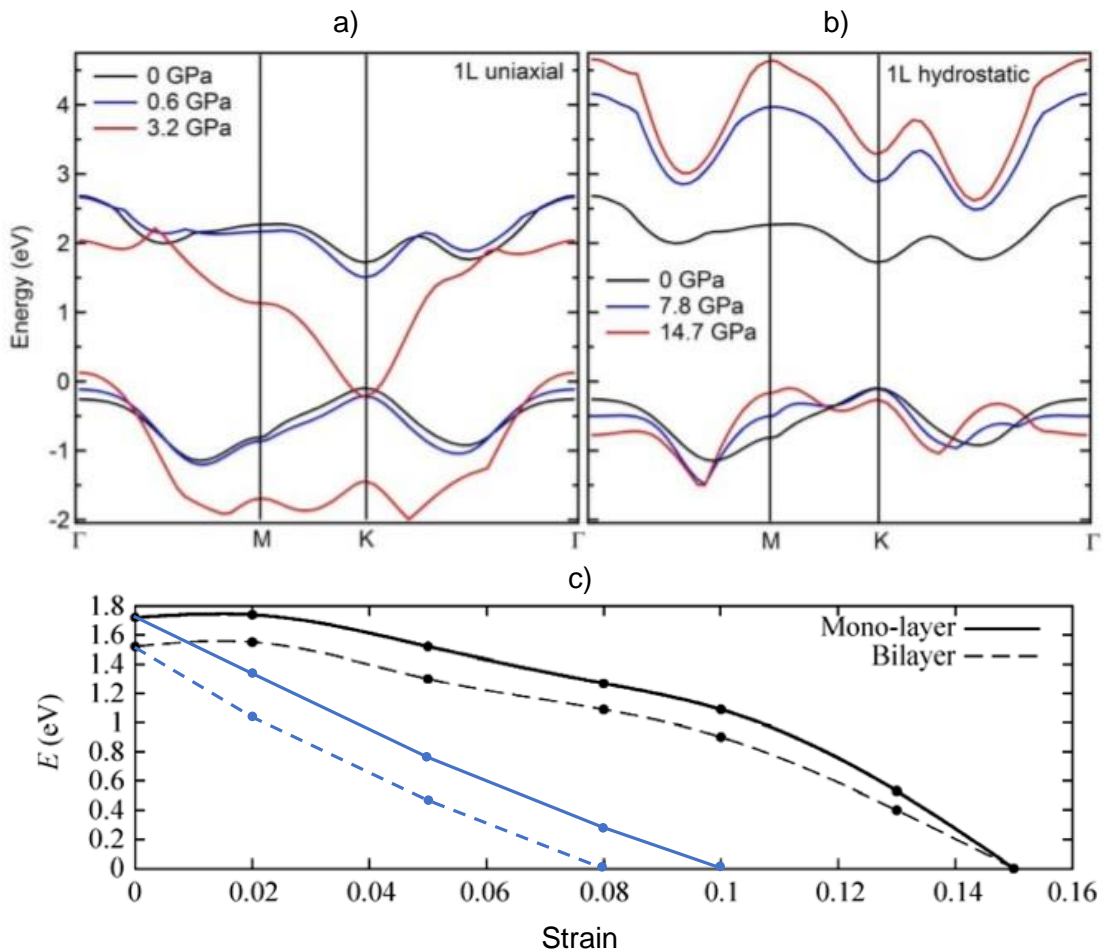
Figure 4: Development of electrical structure of 2D MoS₂ with a) out of plane uniaxial compressive strain and b) hydrostatic strain; c) Changing wideness of bandgap upon applying biaxial compressive (black line) and tensile (blue line) strain. Figure reproduced with permission from: a, b) ref. 31, © 2015 American Chemical Society; c) ref. 32, © Tsinghua University Press and Springer-Verlag Berlin Heidelberg 2011.

By these means, photoluminescence of 2D MoS_2 could be quenched and permitted at will and electric behaviour could be switched from semiconducting to semimetallic and

ultimately metallic. Thus, controlled and reversible application of strain could serve as a tool to modulate MoS_2 properties.

1.2 Molecular/Inorganic Heterostructures

One current direction in electronics and spintronics is to introduce functional molecules to devices in form of single molecules, NPs or thin films and by these means modify or extend the functionality of these devices. Hybrid molecular/inorganic interfaces have already brought some important applications for molecular electronics (such as OLEDs) and recently has begun to be implemented into spintronics.

Among functional molecules, SCO molecules seem to be an interesting choice since they present bi-stability and can be switched between these two states by external stimulus.

1.2.1 Spin-crossover Molecules and Nanoparticles

The SCO molecules are chemical species capable of crossover from a low spin (LS) state to a high spin (HS) state or vice versa as a result of external stimuli, such as temperature, pressure, magnetic field or light.

This phenomenon is explained by ligand field theory which deals with bonding, orbital arrangement, structural features and other characteristics of transition metals' coordination complexes. Transition metals' d orbitals break their degeneracy when placed into non-spherical ligand field, which results in two energetically different levels – t_{2g} (including d_{xy^2}, d_{xz} and d_{yz} orbitals) and e_g (including $d_{x^2-y^2}$ and d_{z^2} orbitals) as displayed in **Figure 5a**. The e_g energy level is higher than the t_{2g} level, due to electron-electron repulsion. The energy difference between these two states is called ligand field splitting (Δ, **Figure 5b**). Another important characteristic for prediction in which spin state molecule will be under given external conditions is the pairing energy (P). This is the spin-pairing energy of electrons within orbital. Depending on the relation between Δ and P, two situations can occur:

- If $P < \Delta$, electrons will prefer to occupy orbitals of subset t_{2g}, which results in LS state.

- If $P > \Delta$, electrons will prefer to maximize spin multiplicity as described by Hund's rule, which results in HS state.
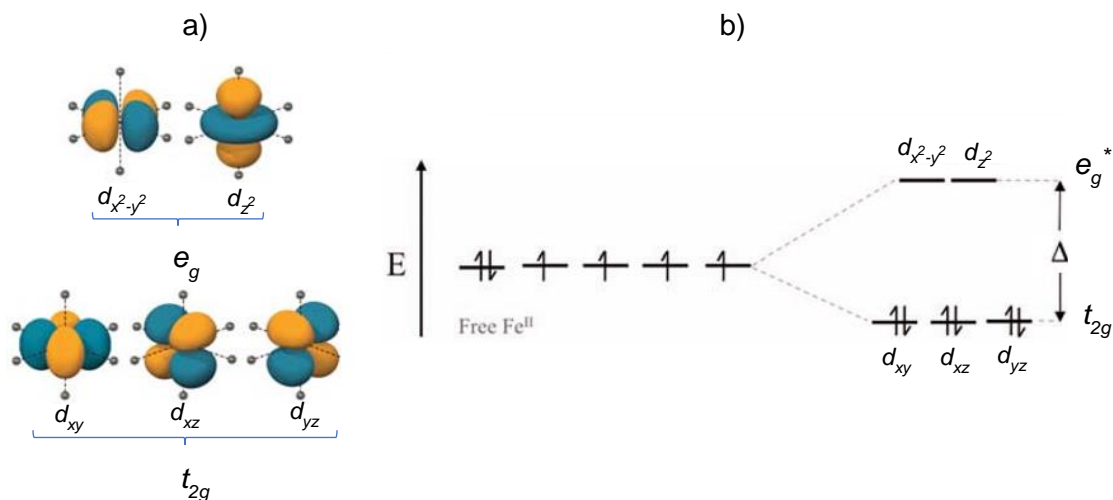
a)   b)

Figure 5: *SCO phenomenon:* ***a)*** *Two groups of d orbitals representing two distinct energy levels;* ***b)*** *Ligand field splitting (Δ).*

In the case of compounds, where $\Delta \approx P$, induction of spin transition is possible through a change of external conditions (light, temperature, magnetic field or pressure) – which is called spin-crossover[33].

One possible way how to introduce SCO functionality into devices is to prepare SCO materials in nanometer size first, i.e. NPs and then integrate them in this form. The most used method to prepare SCO NPs is reverse micelle technique[34] which consists of 4 steps as shown in **Figure 6**. The first step involves the preparation of two separate micellar dispersions upon vigorous stirring at room temperature which enables mixing of different components in the solution (**Figure 6a**) and results in the formation of micelles in a homogeneous medium (**Figure 6b**). During the next step two separate microemulsions are mixed together upon stirring at room temperature. The content of the microemulsion droplets is exchanged by collisions between micelles (**Figure 6c**). Final step consists in destabilization of the micelles upon addition of acetone which promotes the precipitation of the NPs and allows their extraction by centrifugation (**Figure 6d**).

These NPs are interesting for their possible integration into sensing and memory devices since they exhibit bi-stability with the transition between two states through large hysteresis loops which implies memory effects[35].
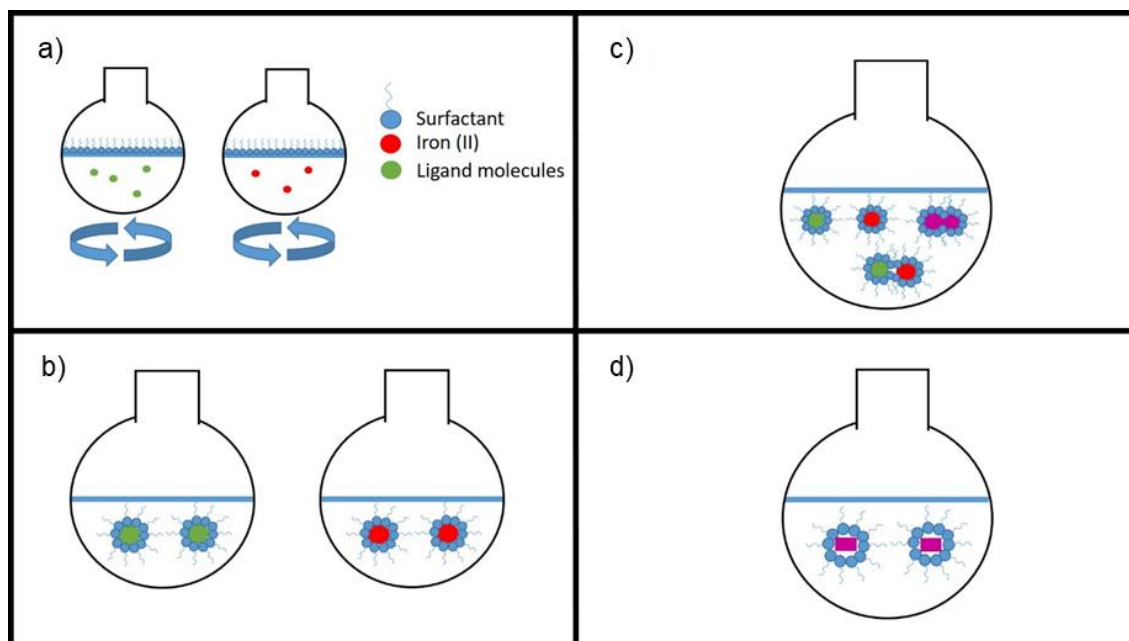
Figure 6: *Reverse micelle reaction scheme:* ***a***) *micelle composition;* ***b***) *microemulsion formation;* ***c***) *micellar exchange;* ***d***) *extraction of formed NPs.*

Exact position of their SCO transition depends on chemical nature of molecules and on size of NPs as can be seen in **Figure 7**. Phenomenon accompanying transition of SCO NPs, such as [Fe(Htrz)$_2$(trz)](BF$_4$).H$_2$O, from LS state to HS state is their change of colour and increase of volume which are result of significant changes in geometry of molecules.[36,37]
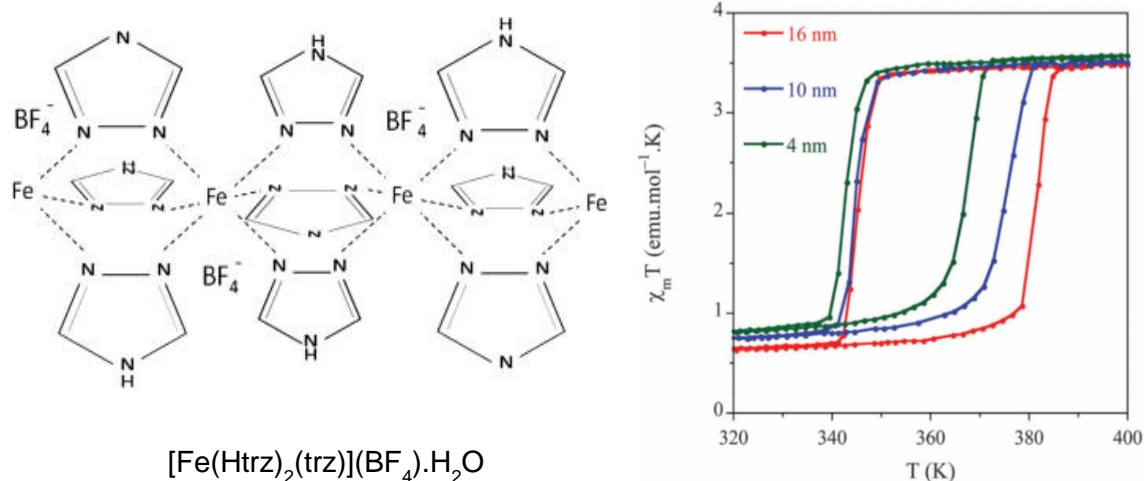
[Fe(Htrz)$_2$(trz)](BF$_4$).H$_2$O

Figure 7: *SCO molecules and NPs: Chain of [Fe(Htrz)$_2$(trz)](BF$_4$).H$_2$O molecules forming NPs; and hysteresis loops for these NPs of various diameters. Figure reproduced with permission from ref. 38. ©The Royal Society of Chemistry 2015.*

1.2.2   Functional Molecules/2D Materials Heterostructures

Surface of 2D materials is ultra-sensitive to its surroundings. On one hand, undesired contaminants from air or solvents used during device processing can cause unintentional change/degradation of electrical properties[39]. On the other hand, this sensitivity can be exploited to modify electronic, optical and magnetic properties of 2D materials with suitable chemical species on demand. Proximity of molecules could modify existing properties of 2D material or even introduce new functionalities. Example of chemical species which are capable to introduce additional functionality to a device are SCO molecules.

In contrast to 2D materials, potentially available in few hundreds, there is almost unlimited number of possible molecules which can be synthetized to fulfil specific needs. Therefore, search for ways of their integration into devices has recently emerged.

One possible way, how to introduce molecules, notional quasi-zero-dimensional building blocks, into devices is to form homogenous thin film on top of 2D material. Molecules are then hold there by vdW, dipole-dipole or electrostatic forces. This non-covalent functionalization of 2D materials is advantageous since covalent modification would introduce defects to crystallographic structure of 2D material and consequently could deteriorate its superior electronic properties. Thin films of functional molecules on 2D material can then serve there as dopants or introduce additional feature.

Doping can be facilitated through charge transfer or dipole-dipole interaction between 2D material and molecular film. Charge transfer is a consequence of energy level alignment between molecules and 2D material. In the case of dipole-dipole interaction, work function of 2D material is shifted as a result of fields emanating from the dipoles acting as a local gate. Although exceptions exist, majority of molecular dopants acts on 2D material in both ways simultaneously[5].

1.3 Device Architectures

In the scope of this thesis, two different device architectures are used:

   i.   Horizontal device architecture
  ii.   Vertical device architecture

1.3.1 Horizontal Device Architecture

In the case of horizontal architecture, current flows horizontally through a device. The device might be constructed from several layers of different materials vertically stacked together, however; determinative is the direction of the current. Different layers of device can have molecular or (nano)particle nature; they can be constructed from 2D materials or bulk components.

It has been already demonstrated that through electrical transport measurements of contacted graphene that is underneath thin film of SCO NPs, it is possible to monitor spin-state switching. As spin-state changes by cycling external stimulus, such as temperature, the electrical resistance of the 2D material decreases and increases in hysteresis loops[40]. In this scenario, hybrid SCO NPs/MoS_2 horizontal devices are investigated in this thesis.

$[Fe(Htrz)_2(trz)](BF_4).H_2O$ SCO NPs were chosen by us to functionalize MoS_2 since their synthesis with desirable dimensionality is well controlled, and their properties are well known in the ICMOL's laboratory. Namely, our property of interest is their change of volume which accompany spin-crossover. Moreover, they can be grafted using electrostatic interactions between positively charged NPs and MoS_2 surface, activated by *n*-butyllithium to become negatively charged. In this way, homogenous compact thin layers of NPs on surface of MoS_2 can be formed.

As SCO is induced by external stimulus and volume of SCO NPs increases, strain inside thin layer of these NPs increases and is expected to apply strain also to MoS_2 (**Figure 8**). If this mechanism proved to work as expected, strain to 2D material could be reversibly switched through external stimulus which would open a new way how to tune electronic structure of 2D materials.
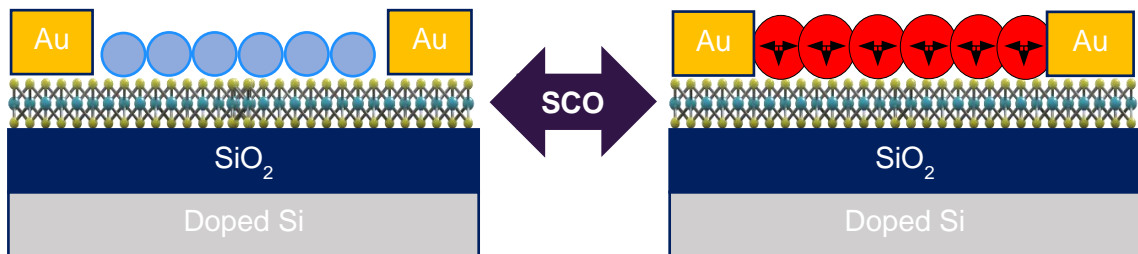

Figure 8*: SCO NPs/MoS_2 heterostructure: Switching of NPs spin-state results in change of volume which could be possibly used to reversibly apply strain to MoS_2.*

In this scenario, we aim to investigate SCO NPs influence on MoS_2 properties where strain effect is expected to influence MoS_2 electrical transport properties (see chapter 2.1).

1.3.2   Vertical Device Architecture

In the case of vertical architecture, electrical current flows perpendicularly to layers of a device across the interfaces of materials which build up these layers. Examples of vertical architectures are some transistor devices (such as tunnelling field effect transistor, band-to-band tunnelling transistor and barristor)[41], and devices for spintronic, such as magnetic tunnelling junction and spin-valve. Since only vertical devices for spintronics are fabricated in the scope of this thesis, only them will be discussed in the following text.

Spintronics (spin transport electronics) is a discipline of solid-state physics, which in addition to charge of electron exploits also its intrinsic spin as information carrier[42]. This gives to the system one more degree of freedom and implicates possibility to construct fast and ultra-low-power non-volatile devices with higher density of data storage[43].

Fundamental spintronic devices are spin-valve and magnetic tunnelling junction (MTJ). They are composed of two ferromagnetic electrodes separated by a non-magnetic spacer as depict **Figure 9a**. In the case of spin-valve, the non-magnetic spacer is a semiconducting or conducting material and serves for spin transport. In MTJ it is an insulator and spin polarized current tunnel through it.

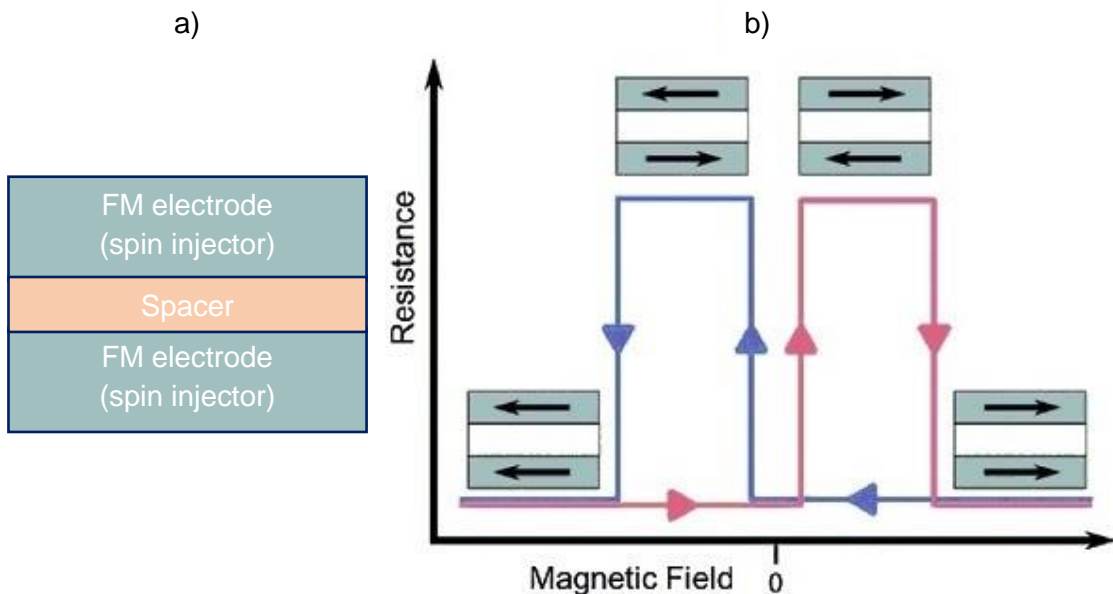*Figure 9: a) Scheme of basic spintronic device; b) Typical measured curve.*

The first FM electrode is used as a spin injector, the spin polarized current is propagated along the non-magnetic spacer and it is detected by the second FM electrode. Depending on the relative orientation of the magnetization direction of the two FM electrodes (parallel or antiparallel) device can be in a low or high resistance state. By applying an

external magnetic field, it is possible to switch between these two configurations. **Figure 9b** shows a typical curve measured in this kind of devices where resistance of the device is recorded while sweeping the magnetic field. This curve is called magnetoresistance (MR) and MR signal is defined as $MR=(R_{ap}-R_p)/R_p$ where R_{ap} is resistance measured for antiparallel configuration and R_p is resistance measured for parallel configuration[44].

Recently, 2D materials and functional molecules have attracted an increasing interest in the field of spintronic as spacer layers.

2D Materials as a Spacer Layer

Atomically thin thickness of 2D materials, the possibility to precisely control their number of layers and the possibility to form thin barriers, free of defects, that offer pinhole-free sharp interfaces, make them ideal building blocks for the construction of spintronic vertical devices. Beyond the use of graphene, in the last years, researchers have focused also on the integration of other 2D materials in MTJ devices[45].

Concerning the large family of TMDCs, promising theoretical calculations were first reported in 2014 by K. Dolui et al. They predicted an extremely large MR signal up to 300 % in Fe/MoS$_2$/Fe MTJ by *ab initio* transport calculations[8]. Some experimental results on MoS$_2$-based MTJ were already successively reported[8,46]. However, amplitude of experimentally observed MR signals reported until now are far from theoretical expectations. One possible cause is that most of reported experimental works were performed in way that bottom FM electrode was exposed to air. Oxidation of FM electrodes is main technological issue of fabrication process that strongly limits MR signals.

In this scenario, our work attempted to integrate MoS$_2$ in MTJ devices as the first step towards the future integration of more complex heterostructures for fabrication of 2D based spintronic multifunctional devices. In our device we take special attention in maintaining high quality non-oxidized interfaces. To do that we started to develop device fabrication using membrane technique where MoS$_2$ flake is deposited over a Si$_3$N$_4$ membrane with a central hole and bottom and top FM electrodes are evaporated on both sides of the flake under ultra-high vacuum (see chapter 2.2). This technique would lead to the formation of clean and oxide free interfaces that are a first step towards the optimization of MR signal in MoS$_2$-based MTJ devices.

Spin-crossover Molecules as Spacer Layer

One current direction in molecular spintronics is to introduce functional molecules to spintronic devices in form of single molecules, NPs or thin films and by these means extend the functionality of these devices. Since SCO molecules present bi-stability and can be switched between these two states by external stimulus, they appear as interesting candidate for such a material to be integrated into spin-valves. Here it would serve not only as spacer between FM electrodes, but also as active switchable component. Then, one could change electrical characteristics of the device through external stimulus in addition to magnetic field. In this scenario, the possibility to introduce SCO molecules into spin-valves are being tested.

One way of integration is deposition of molecules in form of thin films by evaporation technique. Here, SCO molecules are evaporated onto bottom ferromagnetic electrode, preliminary evaporated through first shadow mask with subsequent evaporation of top ferromagnetic electrode through a second shadow mask in cross junction geometry. However, molecules are soft, which lead to easy pinhole formation when top electrode is evaporated and heavy Co atoms with high kinetic energy diffuse through SCO molecular layer until they touch a bottom electrode and, in this way, short-circuit the device. Possible solution of this problem could be previous evaporation of protective layer of lighter molecule which would not penetrate through SCO molecular layer when evaporated and serve as a protective barrier blocking penetration of subsequently evaporated Co atoms. Normally, insulating barriers are being used for this purpose, however, conductive layer of carbon could be also used as suggested by some works[47]. Adding any protective layer has to be, however, accompanied by studies on possible effect of this layer on spin polarization.

Knowing aforementioned, we were developing methods to introduce SCO molecules into spin-valves through the fabrication of cross-junctions using set of shadow masks (see chapter 2.3). Our work especially aimed at validation of this fabrication method itself through preparation of cross-junction with distinct cross bar width and SCO molecular spacer layer thickness, and their resistance measurements to optimize these parameters. Apart from that, effect of carbon layer on possible limitation of short-circuit formation was studied through measured data in comparison with data of cross-junction devices without carbon layer.

2 Experimental Part

2.1 Integration of MoS₂ Functionalized with Spin-crossover Nanoparticles in Transistor Devices

2.1.1 Materials and Methods

Materials

- MoS$_2$ crystal in 2H phase (n-type semiconductor) was bought at HQ graphene. It was synthetically fabricated with a purity of 99.995 % by chemical vapour transport.

- The tape used for mechanical exfoliation was Scotch Nitto tape.

- Solvents used for cleaning were acetone (extra pure), and propan-2-ol (anhydrous 99.5%) provided by Sigma Aldrich and ultrapure water (MQ-H$_2$O, $\rho >$ 18 MΩ.cm) obtained using an Elix-3/Millipore-Q academic water purification system.

- Si/SiO$_2$ substrates were bought at Nova electronic materials. Doped Si (0.001 – 0.005 Ω.cm) has a thickness of 500 μm, and it is covered with 285 nm dry chlorinated SiO$_2$ thermal oxide.

- Cr/Au pre-patterned marker system was prepared on Si/SiO$_2$ substrates using electron-beam (e-beam) lithography and thermal evaporator presented below. Marker system is formed by a matrix of crosses with a mutual distance of 100 μm, and numbers are used for labelling columns and lines.

- Lithography resists 495 PMMA and 950 PMMA were bought at MicroChem.

- Methyl isobutyl ketone 99% bought at Sigma-Aldrich was used for resist development.

- Silver conductive paint used for manual contacting of electrodes to the chip was bought at RS Components.

Methods

- Digital camera Nikon 7000D in combination with microscope Nikon Eclipse LV100D was used to take high-resolution optical images of samples.

- Veeco Nanoscope 4A atomic force microscope (AFM) was used in tapping mode for MoS_2 thickness analysis and surface quality characterization.

- PIONEER Two from RAITH nanofabrication was used for e-beam lithography.

- Edwards AUTO 500 thermal evaporator with a base pressure of 10^{-6} mbar was used for evaporation of electrodes.

- Electric measurements were carried out in MPI ITS150 TRIAX probe station with tungsten probe tips in two points configuration using a Yokogawa GS200 voltage source and Keithley 6517B electrometer.

- Quantum Design PPMS-9 cryostat was used to perform electrical characterization of devices. Measurements were performed in two points configuration with a Keithley 6517B electrometer.

Software

- ImageJ was used for proceeding optical images.

- Gwyddion was used for proceeding AFM images.

- Masks were prepared in AutoCAD2018.

- Igor Pro and Origin Pro 8 were employed for data plotting.

2.1.2   Results and Discussion

To prepare MoS_2/SCO NPs hybrid lateral devices, first, thin layers of 2D material have to be obtained and characterized, followed by e-beam lithography process, evaporation of Au electrodes and functionalization of MoS_2 flakes. The whole process is systematically described step by step in the following text. Finally, representative results of devices measured at probe station and PPMS are presented and discussed.

Exfoliation and Deposition of MoS$_2$ Flakes

First of all, Si/SiO$_2$ substrates with pre-patterned markers were cleaned with acetone, propan-2-ol and MQ-H$_2$O. This soft cleaning procedure was chosen to avoid a damage of pre-patterned markers.
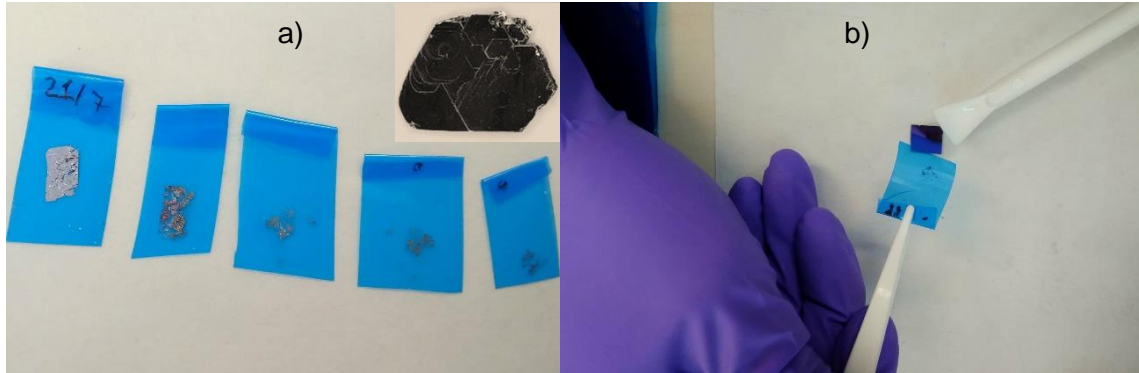

*Figure 10: a) Exfoliation and b) deposition of MoS$_2$ flakes. **Inset**: MoS$_2$ crystal.*

Mechanical exfoliation was performed using scotch tape technique. A special tape, which leaves less glue on the surface of sample than a normal one, was used at this scope. The first exfoliation from bulk MoS$_2$ crystal (**inset of Figure 10a**) was realized. Then multiple peeling from this exfoliated piece of MoS$_2$ crystal was repeated until MoS$_2$ flakes on tape were thin enough (**Figure 10a**). Deposition of MoS$_2$ flakes onto cleaned Si/SiO$_2$ substrate was performed by the last exfoliation step, this time between tape and substrate (**Figure 10b**).

Characterization of MoS$_2$ Flakes

Next step was characterization of samples to select thin layers. First, a screening is realised by optical microscopy (OM). This technique is easy, reliable and, in comparison with other characterization methods, such as Raman spectrometry or AFM, it is a quick way to identify the thickness of 2D layers over a substrate using the optical contrast between flakes and substrate. The contrast varies as number of layers of 2D material changes, due to the increased optical path and higher opacity and can be theoretically predicted employing model[48] based on Fresnel's law. For characterization of MoS$_2$ flakes, Si substrate with 285 nm thick SiO$_2$ layer was used since this thickness gives an optimized contrast between thin MoS$_2$ flakes as a function of their number of layers[49].
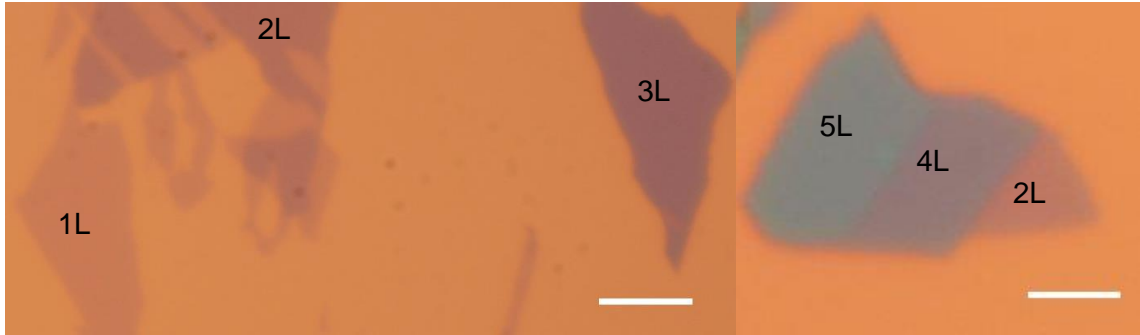
Figure 11: Optical images of MoS₂ flakes - identification of number of layers (nL) using contrast. Scale bar 5 μm.

For the preparation of our devices, the most suitable flakes were the thinnest ones since strain effect of NPs is expected to influence mostly superficial layers of MoS_2, thus, if present, underneath layers could decrease signal of measured effect. **Figure 11** shows how the colour of flakes changes with their thickness. The thinnest flakes have a violet colour, while thicker ones have a blue colour and the thickest yellow colour (**Figure 12**).
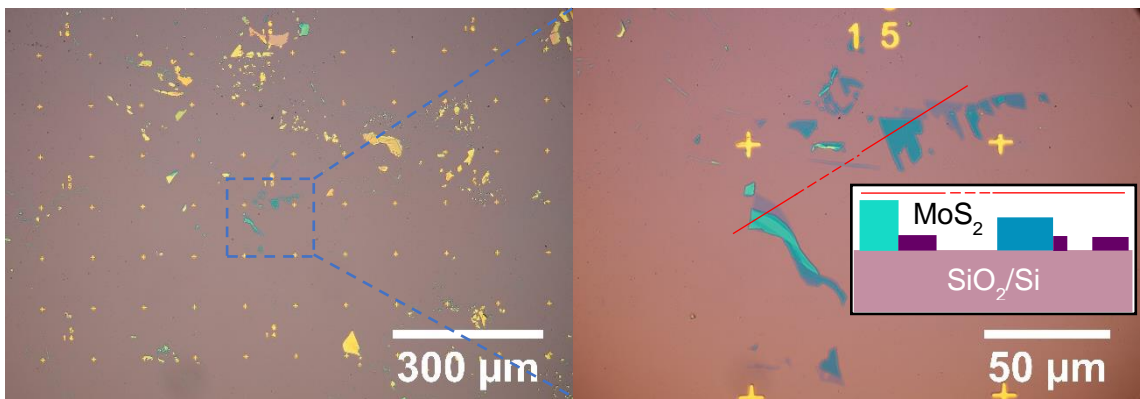

Figure 12: Optical images of the zone with thin MoS₂ flakes over the SiO₂/Si marked substrate. Inset represents schematic profile of substrate with flakes of MoS₂ on it taken over red line.

After all suitable flakes were localized, they were carefully characterized by AFM. Tapping AFM images give information about the topography of flakes, about their possible degradation state (mostly caused by oxidation), cleanliness of samples (e.g. the presence of eventual glue contamination after exfoliation) and flakes thickness. **Figure 13** represents examples of dirty and degraded flakes.
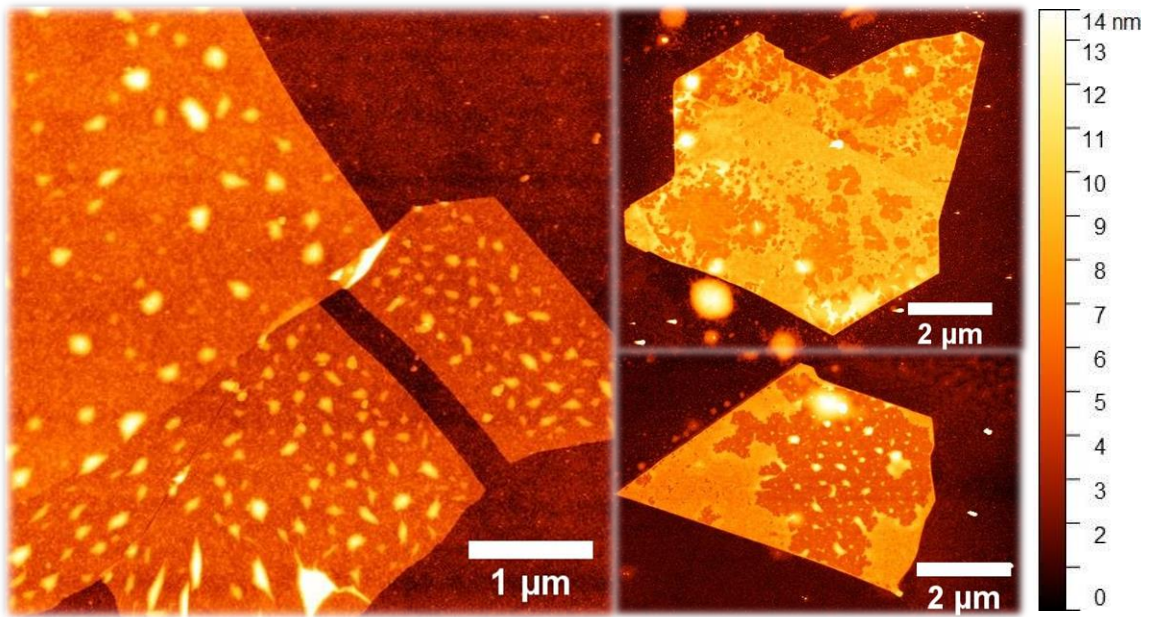
Figure 13: Dirty and degraded MoS₂ flakes.

Figure 14 displays one chosen flake with clean, flat surface, and its profile. The profile was fitted to estimate flake thickness. The thickness of this flake is about 1.5 nm which correspond to two layers of MoS_2. Bilayer MoS_2 flake was measured to determine an RMS roughness of ~ 0.3 nm which indicates a very flat, high-quality surface.
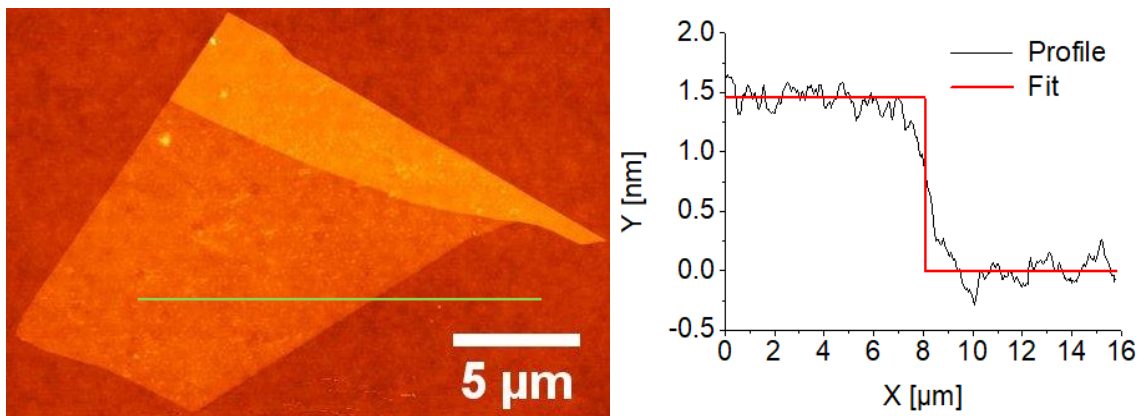

Figure 14: Selected MoS₂ flake and its profile. The green line represents section over which profile was measured.

Device Preparation

Once MoS_2 was mechanically exfoliated over the Si/SiO_2 surface with a pre-patterned marker system and characterized by OM and AFM, next step was preparation of devices

to measure transport properties of the flakes. Scheme of all preparation steps is displayed in **Figure 15** and the following text describes each step more in detail.
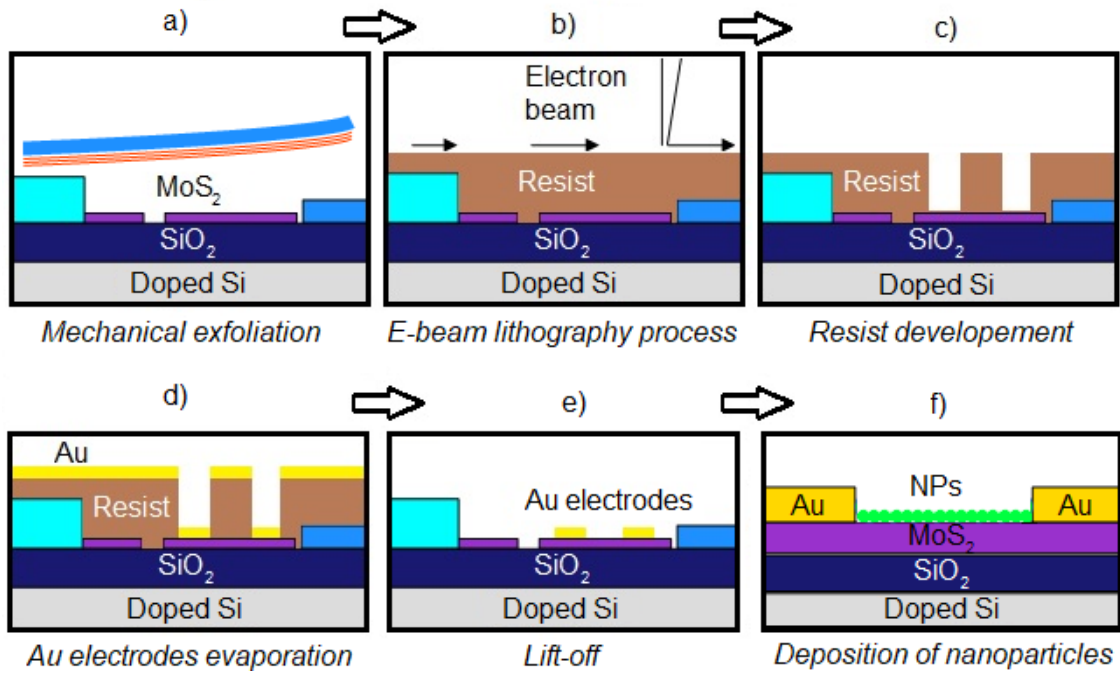

Figure 15: Schematic of MoS$_2$/NPs device fabrication process.

Before starting the lithography process itself, the mask with electrodes were drawn over the selected flakes using software AutoCAD. We used a marker system to determine flakes position over the substrate as shown in **Figure 16**. Electrodes with a gap of about 1.5 µm were drawn over the selected flakes and circular pads with a diameter of 400 µm were drawn in order to be able to manually contact the junction to a chip for PPMS measurements. The prepared mask was loaded with lithography software in the e-beam system.
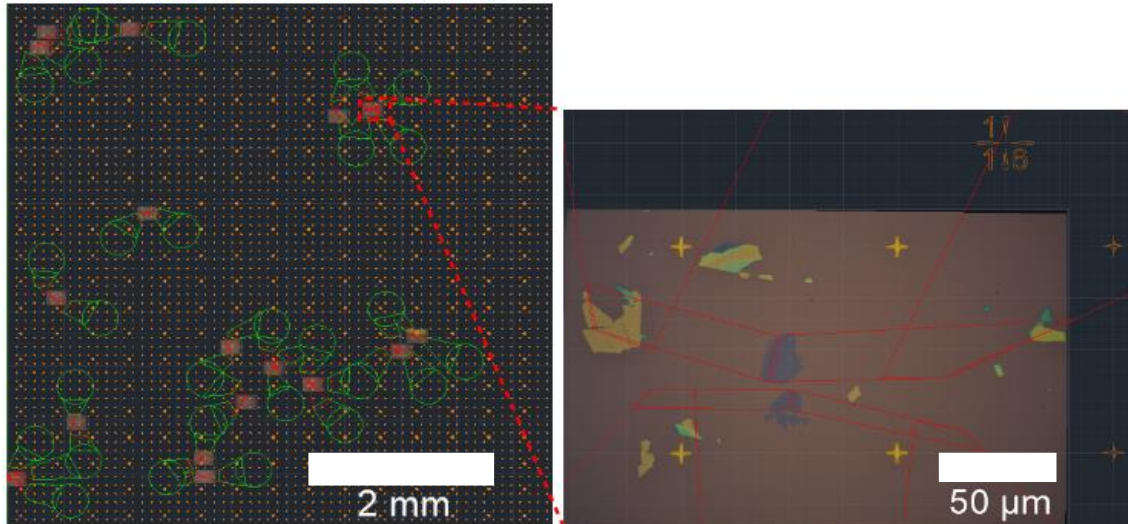
Figure 16: Electrodes drawn over flakes in AutoCAD software.

The first step of the lithography process is to spin-coat samples with a double layer of resist. This is done to facilitate the lift-off process. The sample was placed on a spin-coater and 495 PMMA resist was spin-coated over it at a speed of 2000 rpm for 40 seconds and resist was baked by heating at 180 °C for 7 minutes. Then, a layer of 950 PMMA was spin-coated at a speed of 3000 rpm for 40 seconds and resist was baked as before at 180 °C for 7 minutes.

Next, the sample was inserted into the vacuum chamber of e-beam equipment and lithography was performed (**Figure 15b**). Electron beam writes the pattern of electrodes following the drawn mask. Since positive resist was used, solubility of the zones which are exposed to electron radiation increases.

After removal of the sample from the vacuum chamber, resist was developed by dipping sample into a solution of methyl isobutyl ketone and propan-2-ol (1:1) for 30 seconds and subsequently cleaned in propan-2-ol for 15 seconds. This step removed the resist exposed to electron beam (**Figure 15c** and **Figure 17**).
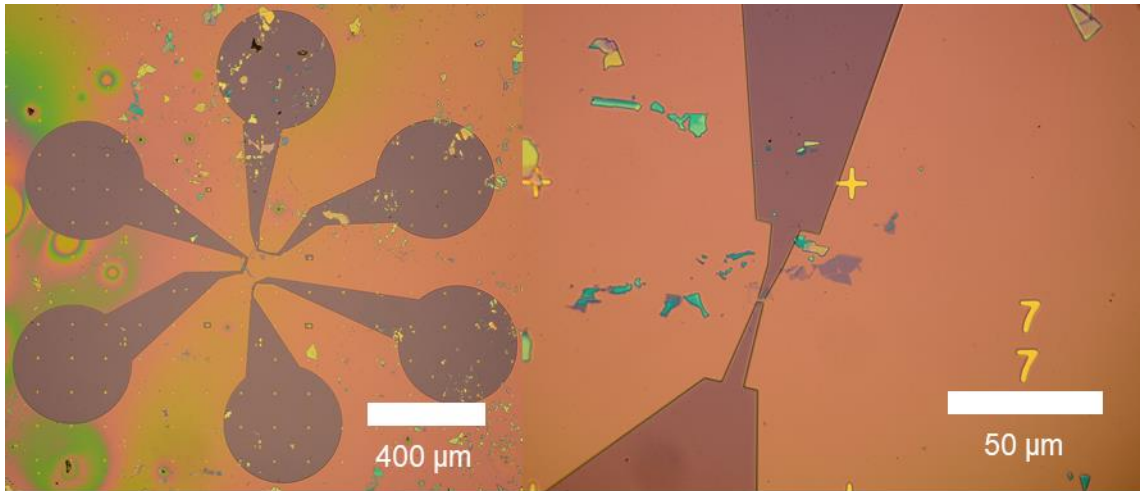
Figure 17: Optical images of sample after development of resist.

Further, 5 nm thick layer of Ti and 50 nm of Au were thermally evaporated (**Figure 15d**). Ti layer serves as an adhesion layer and was added since gold has a poor affinity to SiO_2 substrate and it would be easily removed.

Finally, lift-off was performed by dipping the sample into acetone for approximately one hour. In this step the remaining resist together with Au over it were removed and only drawn Au electrodes remained on the sample (**Figure 15e**).

Final devices were checked by an optical microscope to confirm that flakes were well contacted with electrodes. **Figure 18** shows that electrodes are well positioned over the flakes and that they are not broken.
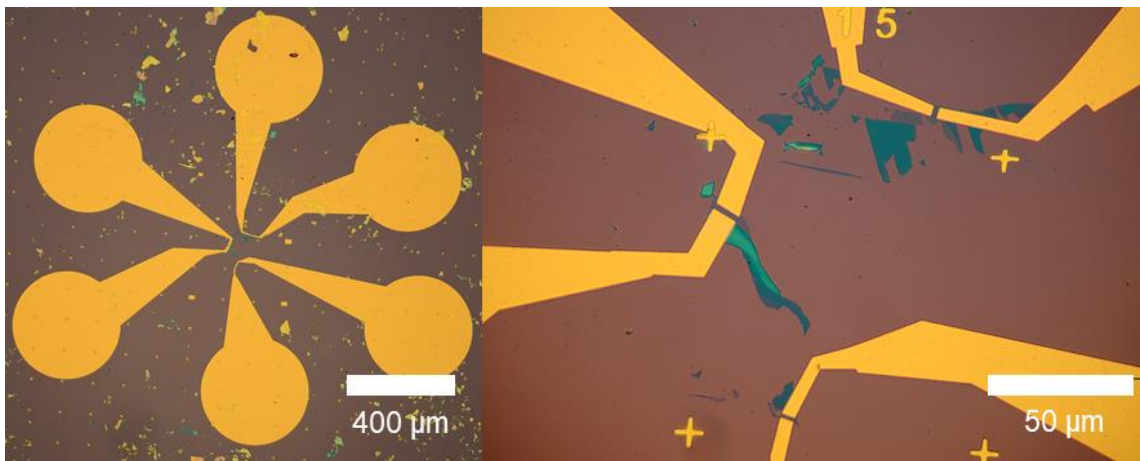

Figure 18: Optical images of evaporated electrodes.

Devices were then preliminarily electrically characterized at probe station. **Figure 19a** shows a schematic of prepared MoS_2-based lateral transistor plugged by probe tips in two points configuration, applying a back gate.
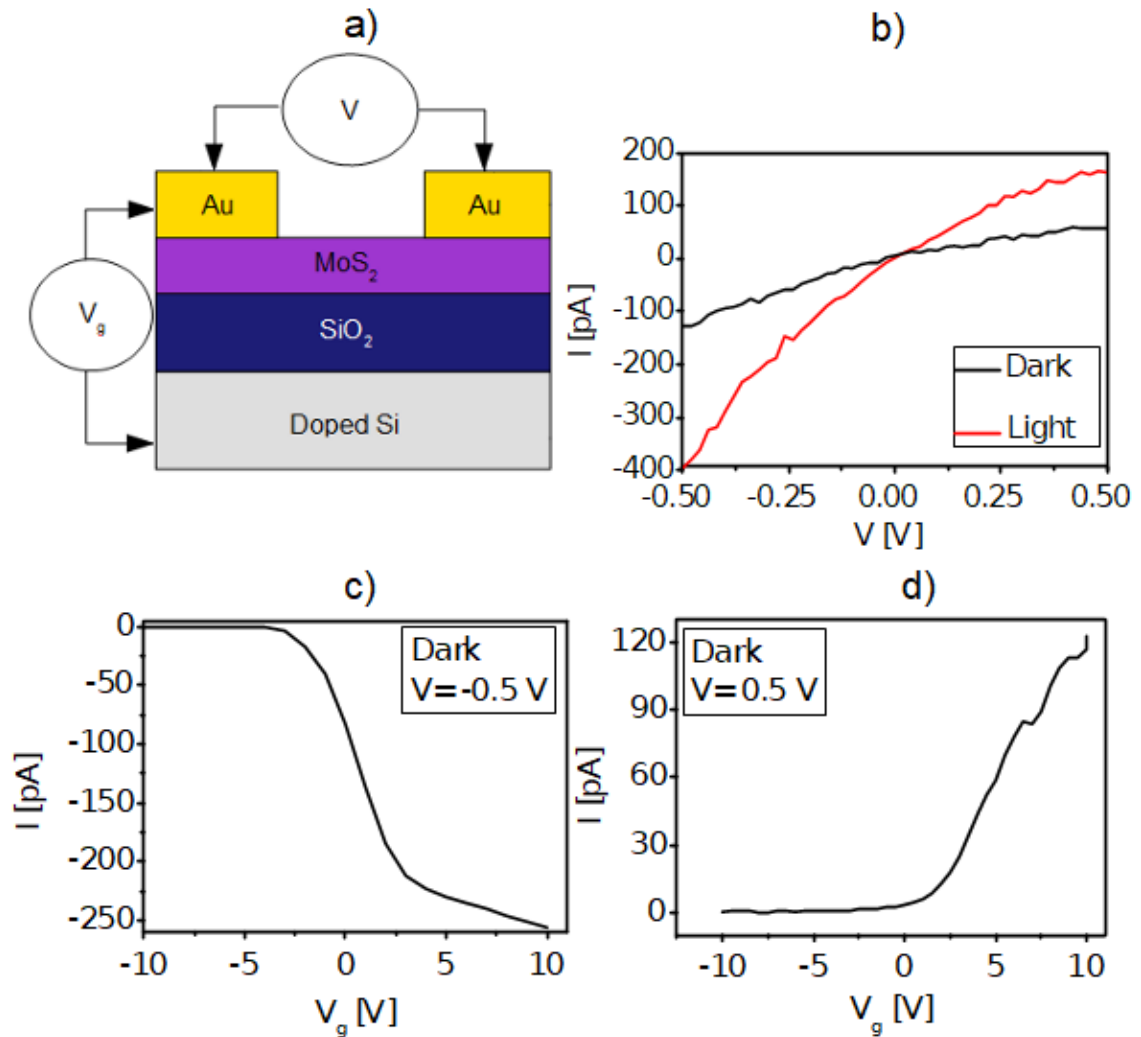
*Figure 19: Probe station measurements: **a**) Scheme of the final device plugged by probing tips; **b**) IV curves for sample in dark and light environment; **c**) Gate-voltage modulation of current in dark environment for source-drain voltage V= -0.5 V and **d**) V= 0.5 V.*

Figure 19b shows IV curves collected at room temperature in dark and under illumination of the sample with white light. Source-drain voltage was applied in a range from -0.5 V to 0.5 V. We observed an increase of current with light.

Then, we also applied a back gate in a range from -10 V to 10 V with a stable value of source-drain voltage of 0.5 V and of -0.5 V respectively (**Figure 19c, d**). We observed a modulation of current with back-gate.

This confirms that our system is working properly, showing expected light and back-gate modulation, and we can proceed to surface functionalization of contacted MoS_2 flakes with SCO NPs.

The synthesis of the [Fe(Htrz)$_2$(trz)](BF$_4$).H$_2$O SCO NPs with size of approximately 4 nm was performed following previously reported method[50] and then deposited onto MoS$_2$ flakes (**Figure 15f**) by a PhD student, whose research is focused on it. **Figure 20a** shows AFM image of SCO NPs forming uniform layer on MoS$_2$ flake. Darker side of the **Figure 20a** is SiO$_2$ substrate where SCO NPs are only randomly distributed without forming compact layer.
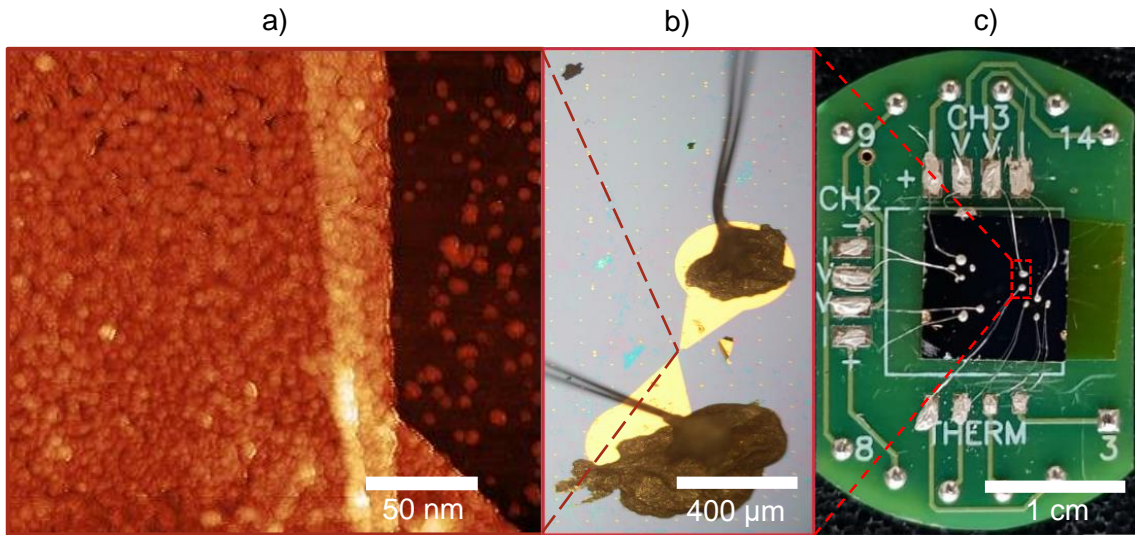

Figure 20: a) AFM image of MoS$_2$ flake functionalized with SCO NPs; b) Detail of the contacted electrodes; c) Sample contacted to the chip.

After functionalization, sample with devices was manually contacted with Ag conductive paint to the chip (**Figure 20b, c**) and measured at PPMS.

First, IV curves at low temperature (280 K) and then at high temperature (400 K) were measured to see if the device is working, applying a voltage from -0.5 V to 0.5 V (**Figure 21a**).

Then temperature dependent measurements were performed with the step of 5 K/min. **Figure 21b** shows how current through the device changes when heating up and cooling down the system in range from 280 K to 400 K. While heating up, we observe two changes in slope of the curve. The first change is observed at 340 K where current begins to slightly decrease. This change is probably caused by smaller SCO NPs whose SCO transition happens at lower temperatures. Minority fraction of smaller (and bigger) NPs than 4 nm is always present in the mixture. The second change occurs at 360 K where SCO transition is expected for 4 nm NPs[38]. Initial decrease of current could be result of small compression strain (up to 2 %) which causes increase of bandgap[32]. As heating continues and strain further increases (above 2 %), the second change in slope can be

36

seen. While cooling down, we do not observe a clear sign of transition, probably due to a gradual change from HS state to LS state.

One unfunctionalized device was also measured for drain-source voltage V = 500 mV at PPMS as reference to have an idea how conductivity of MoS_2-based transistor changes with temperature. **Figure 21c** shows, that current through MoS_2 flake increases with increasing temperature as expected for semiconductor whose conduction band is thermally populated. However, in this case we do not observe any change in slope of the curve.
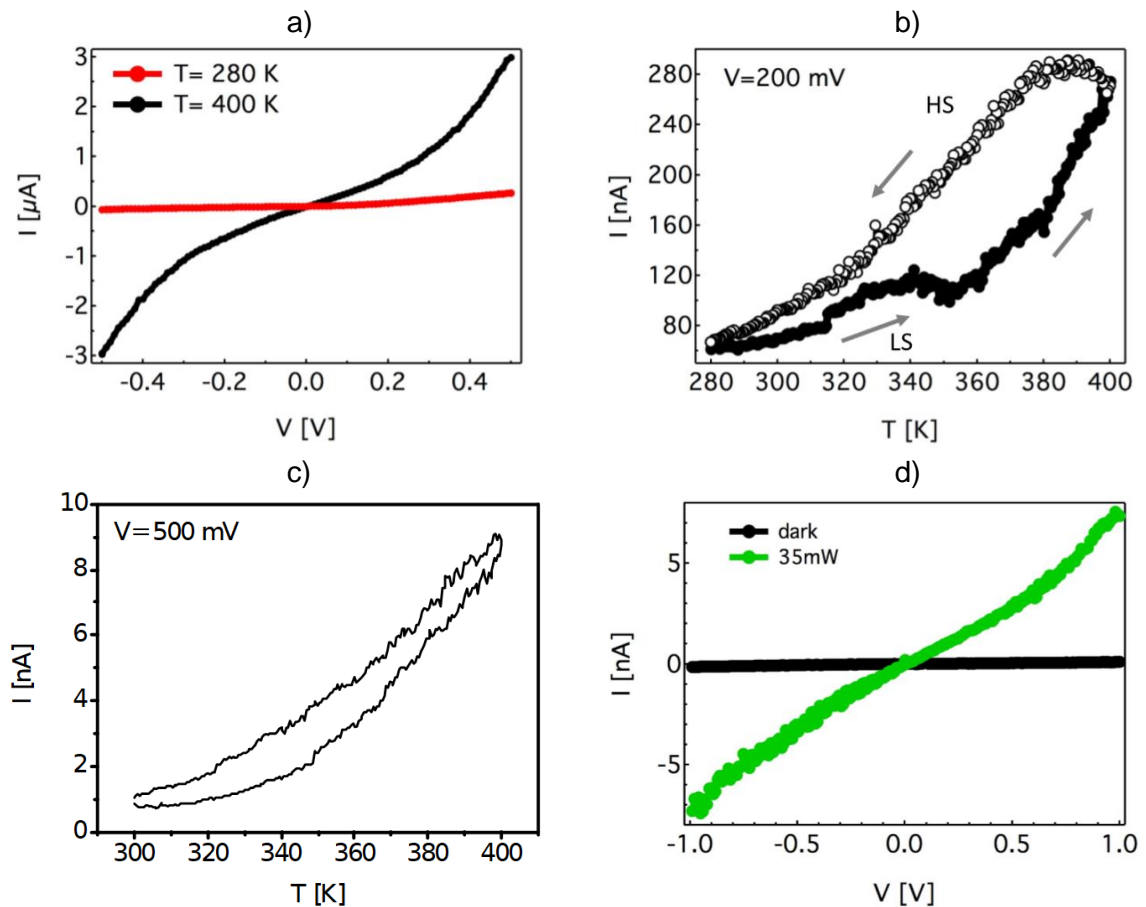
*Figure 21: PPMS: **a)** IV curves of functionalized MoS₂ at 2 distinct temperatures; **b)** Modulation of current with temperature for MoS₂ functionalized with SCO NPs and **c)** for MoS₂ alone; **d)** Modulation of current in dark and light environment.*

The current through MoS_2 flake is also one order of magnitude lower compare to functionalized device, despite applying higher voltage. This can be result of SCO NPs pressure on MoS_2 as they lie on top of it or result of a doping effect. Hysteresis observed in MoS_2 FET alone is probably caused by charge trapping at the interface with SiO_2/Si substrate and absorption of moisture and gases on surface of MoS_2 as suggested previous works[51].

We also started to investigate current modulation with light. In **Figure 21d** we show current change when irradiating sample with green laser (35 mW) at room temperature changing voltage from -1 V to 1 V. For sample in dark, we observe a lower current as expected for semiconductor.

Figure 22a shows current modulation when sample was irradiated with the same green laser in pulses of duration 200 s with stable drain-source voltage of 1 V. With growing number of ON-OFF cycles, immediate ON-current, after switching the laser on, reached higher value. This can be attributed to growing population of SCO molecules switched to HS state.
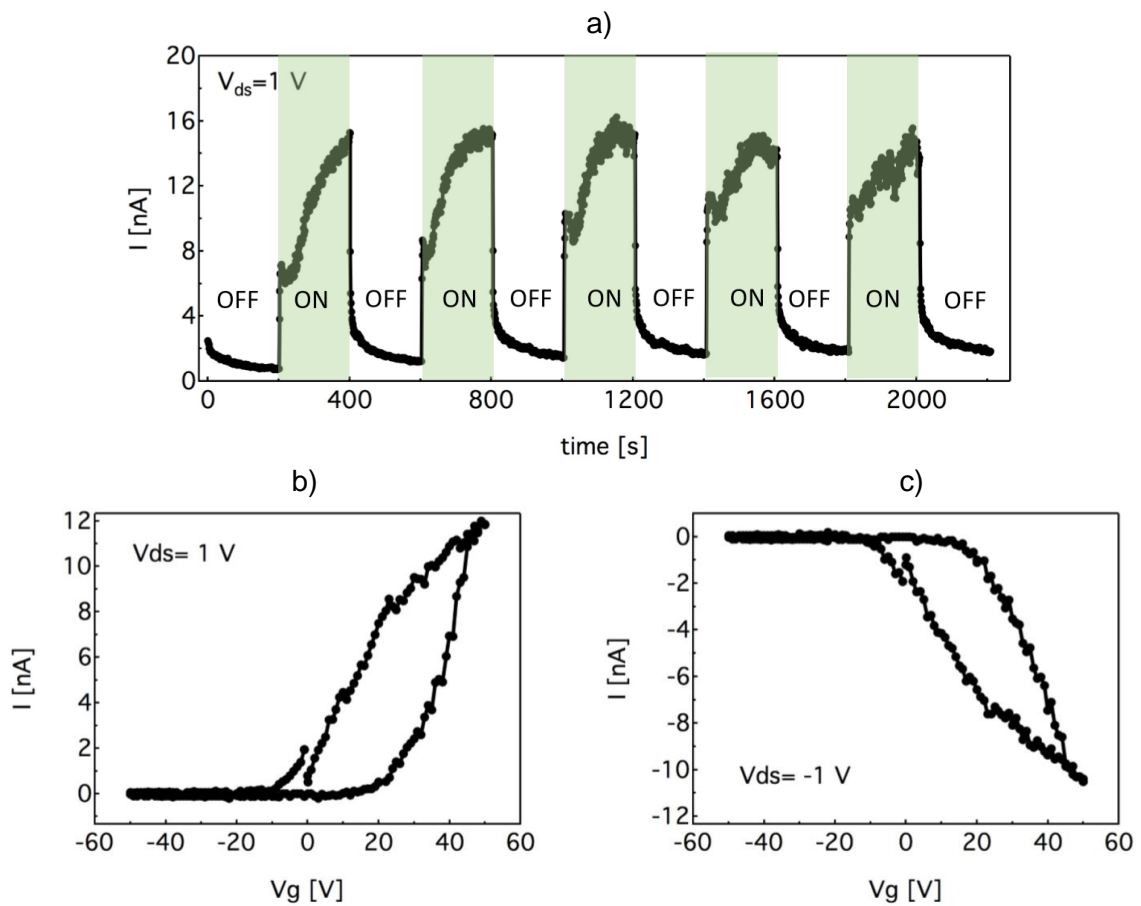
Figure 22: PPMS: a) Current measurement of functionalized MoS₂ under laser irradiation in pulses; Gate-dependent modulation of current at drain-source voltage b) V=1 V and c) V= -1 V.

In addition, gate-dependence was investigated. IV curves were obtained for stable drain-source voltage of V= 1 V (**Figure 22b**) and of V= -1 V (**Figure 22c**) changing back-gate voltage in a range from -50 V to 50 V. Modulation of current with back-gate was for positive and negative source-drain voltage almost identical.

In total, we have exfoliated 17 samples. Two samples did not provide any usable flakes. From 3 to 12 flakes per each sample were selected to contact them with electrodes. One sample was lost since it was not possible to spin-coat the resist over its surface. Other problems with e-beam lithography and as consequence during development of resist occurred in the case of 2 samples, which led to failure in forming Au electrodes. Further, some electrodes were also broken, shifted or poorly developed and short-circuited. Few flakes were removed during lift-off step too. Another possible problem causing failure of fabrication process could be contamination of some flakes with polymeric residues from exfoliation tape and resist which results in poor contact of flakes with electrodes.

From those 14 samples, that underwent lithography process, 108 electrodes were evaporated. 76 flakes seemed well contacted, which gives 70 % success rate of lithography process. Roughly 35 devices were contacted to the chip, however, about half of them already resulted too insulating to be measured, while about 10 devices gave some signal and evidence of functionalization.

Measured electrical transport properties of hybrid MoS_2-SCO NPs devices showed change in slope of current through MoS_2 induced by the transition of SCO NPs from their LS state to HS state. One possible explanation of this phenomenon is that increase of NPs volume, as the result of temperature-induced SCO, causes strain to the 2D material. This strain then slightly changes the MoS_2 bandgap, which results in a modification of its electrical properties. Nevertheless, we showed here only preliminary results of measurements of samples since further data and their more detailed analysis are needed to better understand the phenomenon.

2.2 Integration of MoS_2 into Magnetic Tunnel Junction

2.2.1 Materials and Methods

- MoS_2 crystal, exfoliation tape, substrates, MQ-H_2O and equipment for characterization (OM, AFM and PPMS) were the same ones described in chapter 2.1.1.

- Hydrogen peroxide (H_2O_2), solution 30% *w/w* (110 vol), extra pure was provided by Scharlau. Ammonium hydroxide (20% solution) was bought at Sigma-Aldrich.

- Stamp for flake transfer is a glass microscope slide with a piece of a transparent polymer at one end (polydimethylsiloxane (PDMS)) that is covered with a thin film of polycarbonate (PC).

- The Si_3N_4 membrane on Si substrate had dimensions of 250 µm x 250 µm and thickness of 200 nm and was bought at TED PELLA. A central hole with diameter of 1 µm was prepared by LMA laboratory of University of Zaragoza using Dual beam Helios 600/650.

- Thermally resistive Kapton tape was used as shadow mask during electrode deposition.

- MBE evaporator (with base pressure of 10^{-9} mbar) from CREATEC was used for electrodes evaporation.

2.2.2   Results and Discussion

Exfoliation, deposition and characterization steps of vertical device fabrication were exactly same as those presented in subchapter 2.1.2, therefore only differences in cleaning procedure and parameters of flakes selection are discussed in following text. **Figure 23** shows schematic of vertical device fabrication process and each step is explained more in detail in following text.
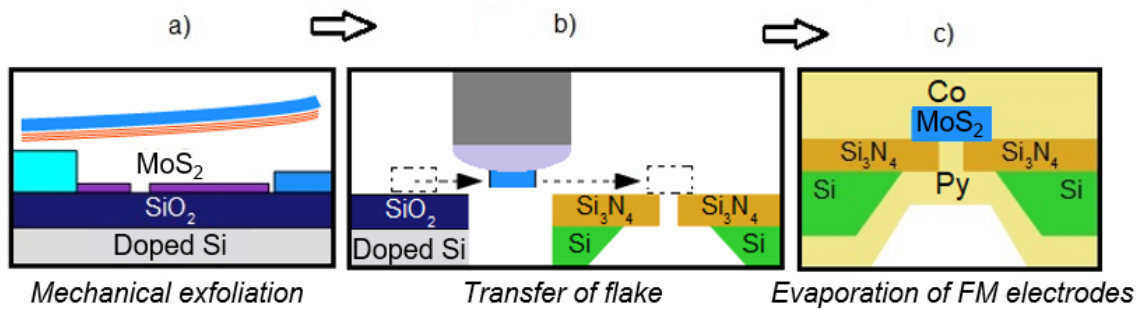
Figure 23: *Schematic of vertical device fabrication process.*

First of all, Si/SiO$_2$ substrates were cleaned through 3 sonication cycles in NH_3OH: H_2O_2: MQ-H_2O (1:1:2) solution and an additional 3 sonication cycles in pure MQ-H_2O with duration of 10 minutes each cycle. This hard cleaning procedure could be performed since substrates were used only to obtain thin flakes, therefore one does not have to be afraid of damaging SiO$_2$ which is, in comparison, indeed crucial in the case of fabrication of transistors (chapter 2.1). Then, thin MoS$_2$ flakes were mechanically exfoliated and deposited onto cleaned substrates in the same way as in chapter 2.1.

Since maximal value of magnetoresistance was predicted for spacer of 7 MoS_2 layers[8], flakes with a thickness around 6 nm were selected and characterized by AFM (**Figure 24**).

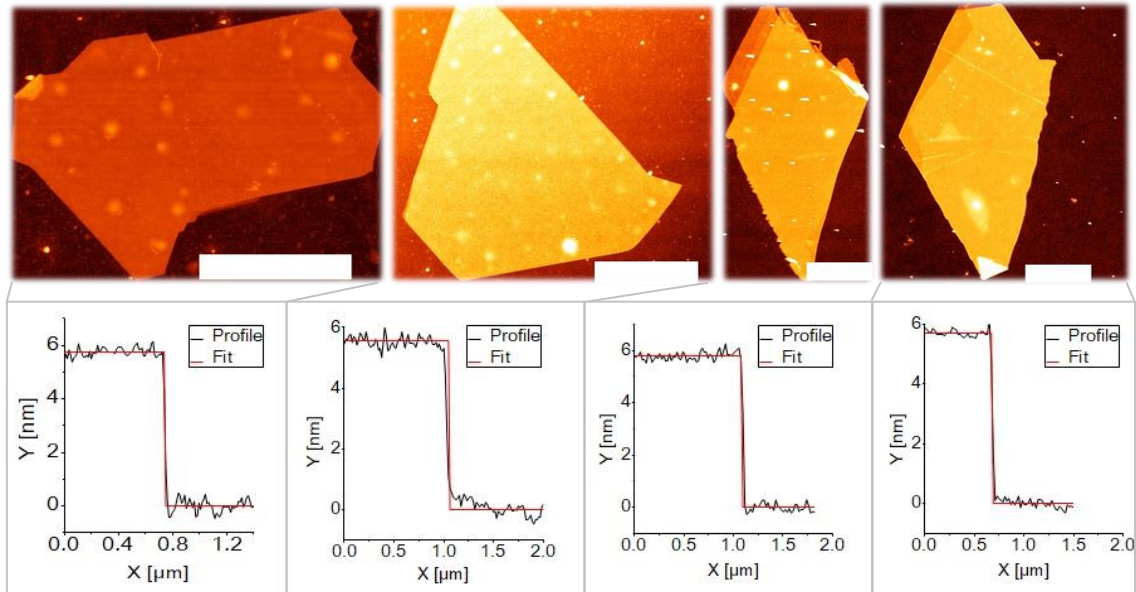*Figure 24: AFM pictures (top) of selected flakes and their profiles (bottom). Scale bar 3 µm.*

Then, selected flake had to be positioned over a 1 µm central hole in a Si_3N_4 membrane. Si_3N_4 serves as an insulating support while FM electrodes are evaporated on both sides of it.

The transfer of flakes was realized using a home-made pick up station (**Figure 25a**) with help of PhD student who assembled it. With this equipment combined with OM, it is possible to precisely control distance between sample placed on table and mechanical holder with a stamp - a sticky polymer on glass slide. All transfer is divided into four steps (**Figure 25b-f**):

1. PDMS/PC stamp is first put in contact with intended flake with the help of a 3-axis micromanipulator and the polymer heated up to 110 °C for 10 minutes, which leads to an increase of its fluidity and melt polymer stick to the sample. Temperature is then decreased, and the polymer starts to return to its original solid state (**Figure 25b**).

2. When the temperature is around 55 °C, the stamp with the flake are separated slowly from the substrate (**Figure 25c**).

3. Further, the sample is removed and the Si substrate with the Si_3N_4 membrane is placed on the sample holder (**Figure 25d**). Hole in the membrane is found and

stamp with the flake is positioned over it. Temperature is increased up to 180 °C; the PC melts and attaches to the substrate (**Figure 25e**).

4. The stamp is removed slowly, and the PC is dissolved in chloroform, leaving the flake attached in the desired location of deposition (**Figure 25f**).
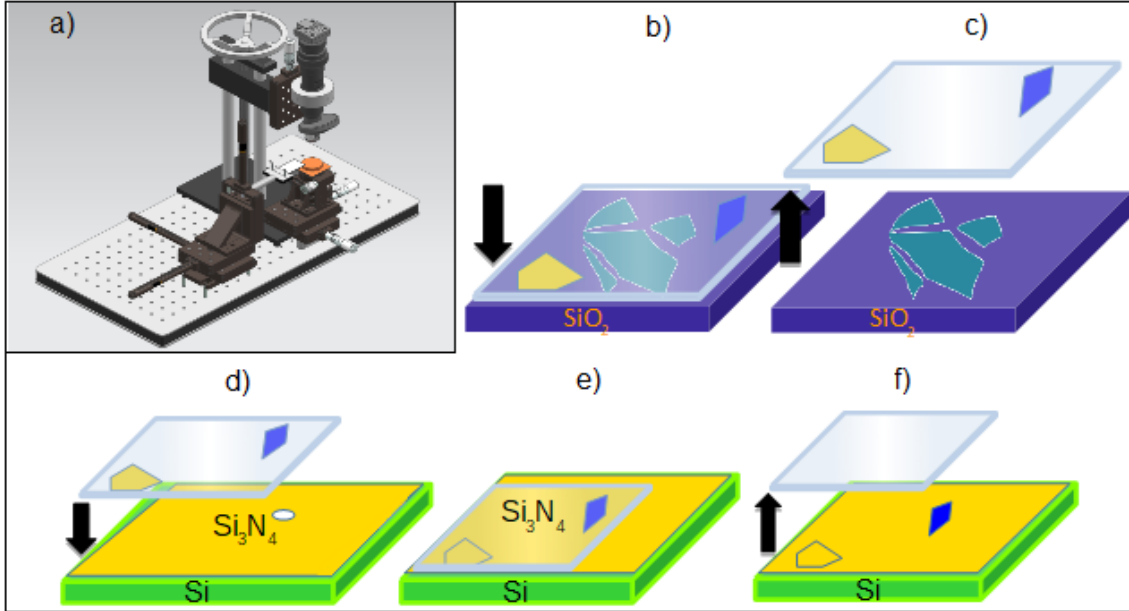
Figure 25: a) Pick up station; b-f) transfer process.

This transfer process is particularly critical device fabrication step since risk of flake damage and/or membrane break is high. In our case, we lost 3 flakes and 4 membranes before successful transfer was performed.

Optical image of transferred flake over the hole in the membrane is displayed in **Figure 26**. For the purpose of better visibility of flake and underneath hole, their borders were highlighted with red and black marker line, respectively.

Figure 26: Optical images of MoS$_2$ flake over 1 μm hole in Si$_3$N$_4$ membrane on Si substrate.

After the successful transfer process, ferromagnetic electrodes were evaporated on both sides of the flake. The sample was precisely positioned over a hole in the metallic plate which served as a shadow mask for evaporation of one electrode. Further, the sample was

fixed with Kapton tape, into which a circular hole was created to use it as shadow mask for the second electrode (**Figure 27a**).
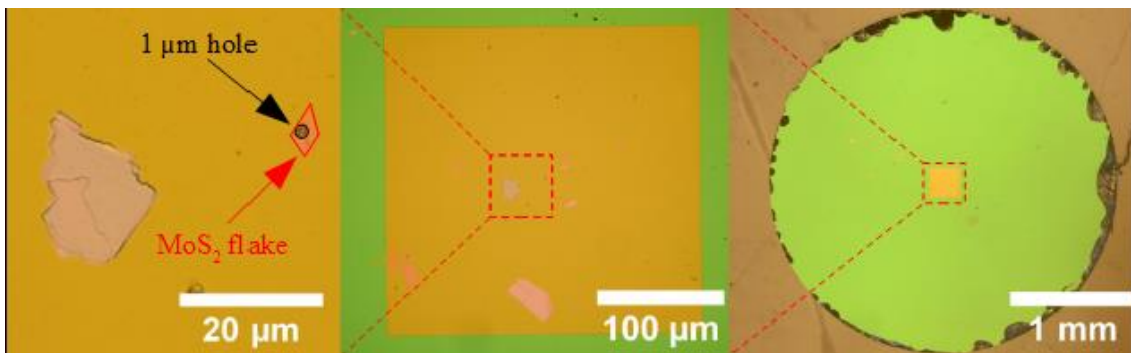
After that, the sample was inserted into a UHV evaporator and 15 nm thick layer of permalloy and 50 nm thick Au capping layer was deposited on one side. The sample was then turned upside down in controlled atmosphere and 20 nm of Co and 70 nm of Au were evaporated as the second electrode (**Figure 27b**). To better understand evaporation process, it is schematized in **Figure 27c, d, e**. The final vertical device was manually contacted to a chip (**Figure 27f**) and measured at PPMS.

Astonishingly, electrical measurement showed that the device was completely insulating which made any further measurements impossible. This must be due to a device fabrication issue. Problem was probably that polymer used for transfer was not completely removed from MoS_2 surface. Another possible issue could be formation of a cavity between flake and FM electrode due to shadow effect while evaporating. This explanation, however, is not very probable since geometry of system (hole diameter to hole deepness ratio of 5:1) does not make it prone to this error. To solve this problem, more devices are needed to be fabricated with special attention to cleaning of the sample to remove the polymer residues from flake after its transfer by an annealing process.
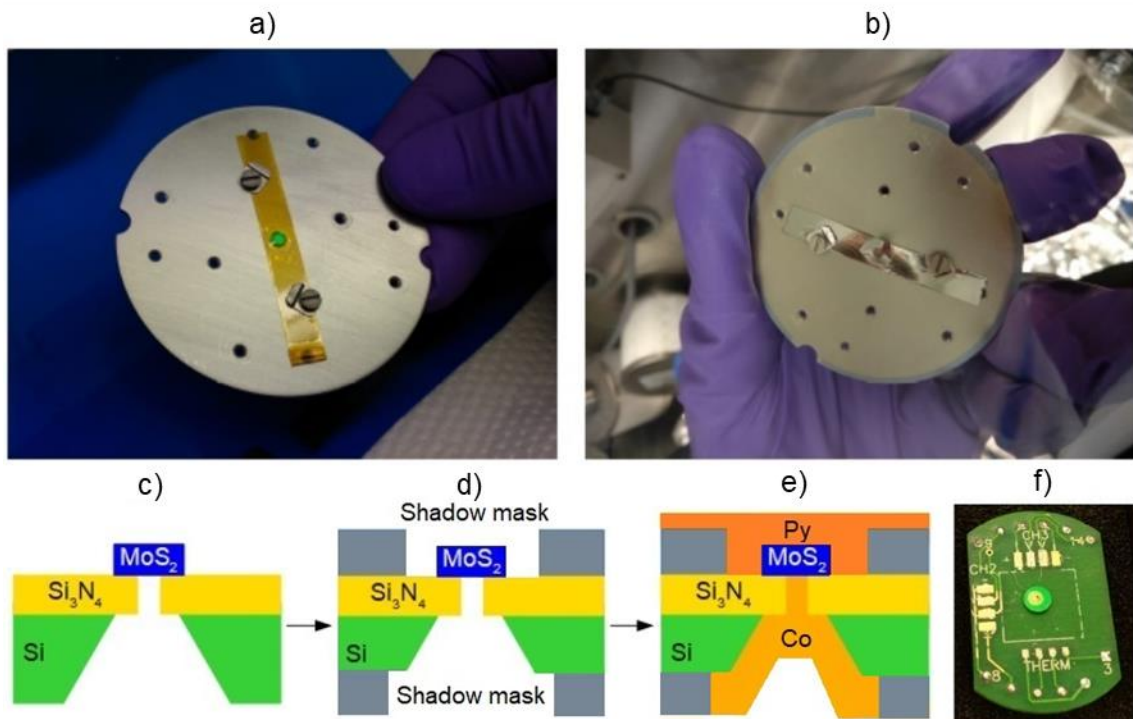

Figure 27: a) Optical images of sample before and b) after evaporation of FM electrodes; c) Scheme of MoS₂ over a 1 µm hole; d) Scheme of shadow mask over MoS2 flake; e) Scheme of FM electrodes evaporation through shadow mask (Py= permalloy); f) Optical image of final device connected to chip for PPMS measurements.

2.3 Integration of Spin-crossover Molecules into Vertical Spin-valves

2.3.1 Materials and Methods

- Two inches Si/SiO_2 substrates were bought at Nova electronics. Non-doped Si (1- 100 Ω.cm) has a thickness of 500 µm and it was covered with 285 nm wet SiO_2 thermal oxide.

- MBE evaporator (with base pressure of 10^{-9} mbar) from CreaTec was used for evaporation of FM electrodes and SCO molecules.

- Mo shadow masks with electrode bars of 50 µm, 100 µm, 500 µm width were implemented into evaporator to deposit electrodes.

- Electric measurements were carried out on MPI ITS150 TRIAX probe station with tungsten probe tips in two points configuration using a Yokogawa GS200 voltage source and Keithley 6517B electrometer.

2.3.2 Results and Discussion

Electrical resistance of cross-junction vertical molecular devices with different spacer thickness was measured to test possibility to obtain short-circuits-free junctions and find an optimized thickness. Fabrication process of these devices is described in following text.

Wafers with vertical devices from SCO molecules were prepared in following way:

a. First, two inches wide SiO_2/Si wafer was placed inside the metal evaporation UHV chamber and a layer of permalloy (NiFe alloy; 80:20) was deposited through a shadow mask to fabricate bottom electrodes bars with width of 50 µm, 100 µm and 500 µm.

b. Subsequently, the mask was removed, and wafer was moved to the molecular evaporator chamber without breaking vacuum and a layer of SCO molecules was deposited over the whole wafer with a defined thickness.

c. Then, the wafer was moved back into metal evaporation UHV chamber again without breaking vacuum, and carbon protective layer was deposited with a defined thickness using a second shadow mask with the bars of 50 µm, 100 µm,

500 μm now oriented 90° regard to bottom electrodes. Finally, cobalt was evaporated as top ferromagnetic electrode in the same chamber using the same mask as for carbon evaporation, which led to the formation of cross-junctions (**Figure 28a**).

SCO molecules were [Fe(H$_2$B(pz)$_2$)$_2$(phen)] complexes (**Figure 28b**), where (H$_2$B(pz)$_2$ is dihydrobis(pyrazolyl)borate and phen is 1,10-phenanthroline. Molecules were deposited with these thicknesses: 60 nm, 20 nm, 10 nm and 5 nm for purpose of finding optimal thickness to obtain thin layers while limiting pinholes formation. Carbon layer was added to test its ability to prevent short circuits and was deposited with thickness of 10 nm.
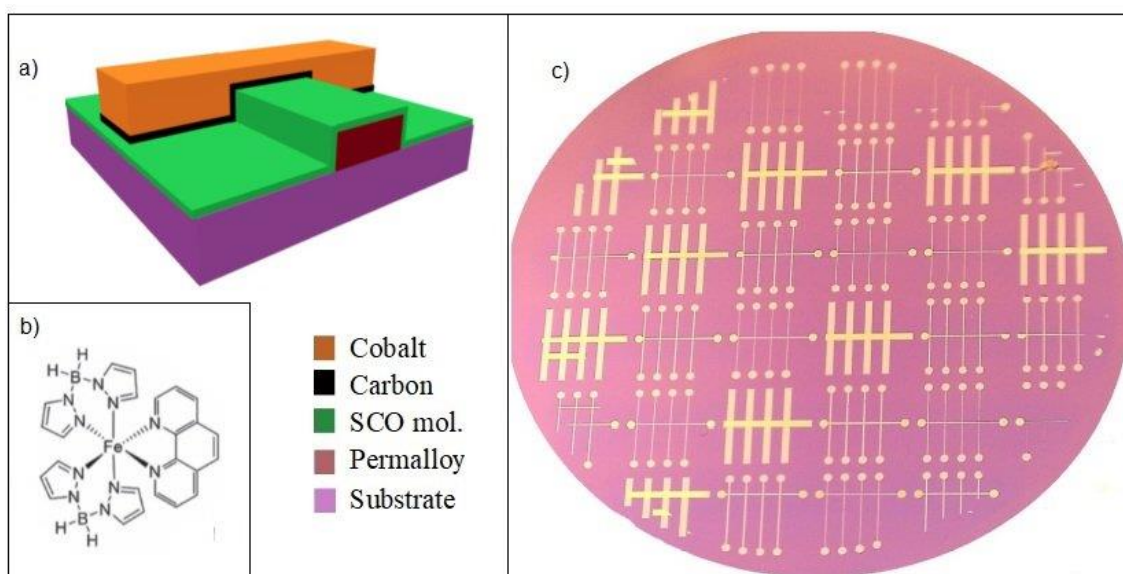
*Figure 28: Vertical device from SCO molecules: **a)** Scheme of SCO cross-junction; **b)** [Fe(H$_2$B(pz)$_2$)$_2$(phen)] complex (SCO molecule); **c)** Optical image of two inches Si/SiO$_2$ wafer with prepared cross junctions.*

Deposition of devices onto wafers through this method is well-reproducible and using set of shadow masks brings advantage in preparation of many devices at the same time (**Figure 28c**). The number of cross-junctions per wafer is approximately 150. Sufficient number of devices per wafer is necessary to have a satisfactory number of measurements for a robust statistic and for higher probability of successful device fabrication.

Four samples of SCO cross-junction devices with carbon layer (see **Table 1** and **Figure 29**) were measured at probe station and compared with data of those two without carbon layer provided by colleague (see **Table 2** and **Figure 30**).

	Thickness of electrodes [μm]	Percentage of junctions measured with given resistance [%]			
		Resistance [Ω]	Resistance [kΩ]	Resistance [MΩ]	Resistance [GΩ]
SCO/C	50	0	0	0	100
60 nm/10 nm	100	0	3	0	97
	500	13	27	12	48
SCO/C	50	0	1	7	92
20 nm/10 nm	100	1	3	3	93
	500	22	37	16	25
SCO/C	50	14	11	43	32
10 nm/10 nm	100	20	8	22	50
	500	61	24	6	9
SCO/C	50	100	0	0	0
5 nm/10 nm	100	100	0	0	0
	500	100	0	0	0

Table 1: *Measured data of devices from SCO molecules with carbon protective barrier.*
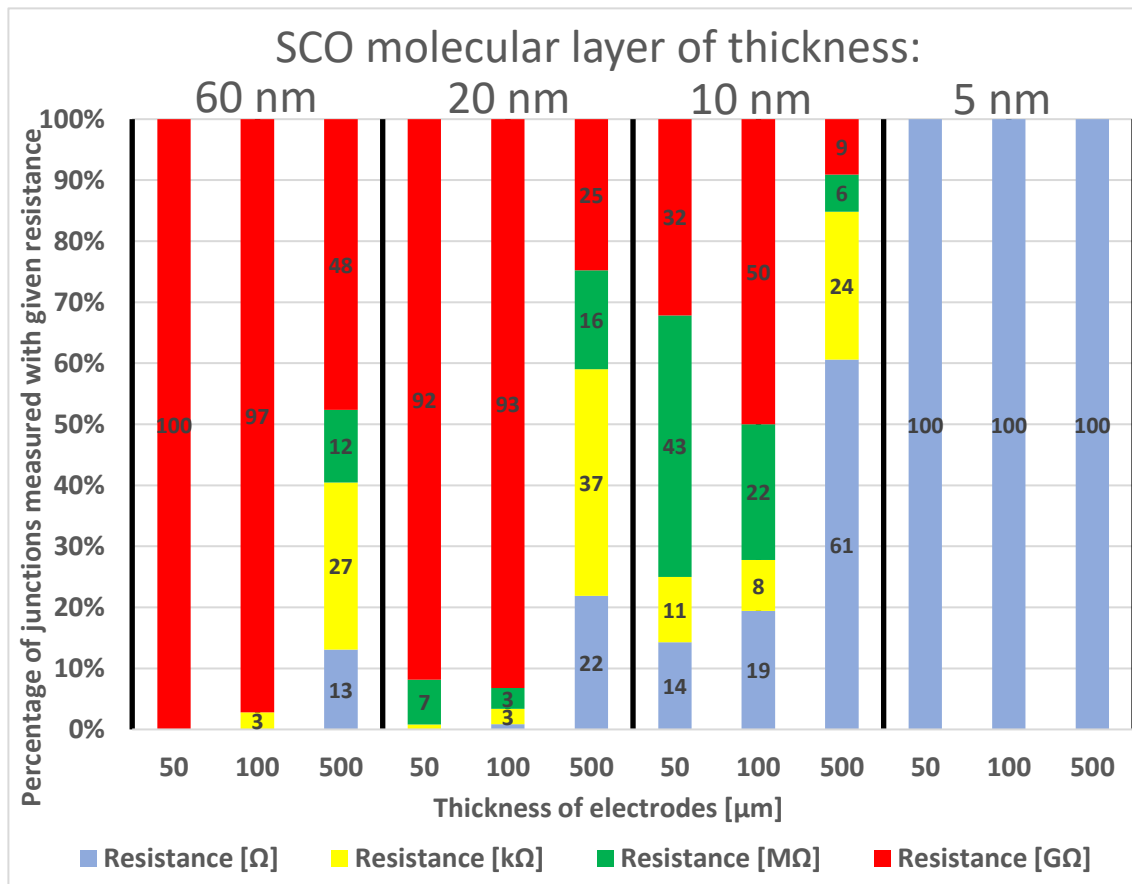

Figure 29: *Graphical representation of statistic measurements of devices with carbon layer.*

	Thickness of electrodes [μm]	Percentage of junctions measured with given resistance [%]			
		Resistance [Ω]	Resistance [kΩ]	Resistance [MΩ]	Resistance [GΩ]
SCO	50	0	0	4	96
20 nm	100	0	3	3	94
	500	34	24	24	18
SCO	50	3	3	3	91
10 nm	100	15	5	12	68
	500	86	14	0	0

Table 2: Measured data of devices from SCO molecules without carbon protective barrier.
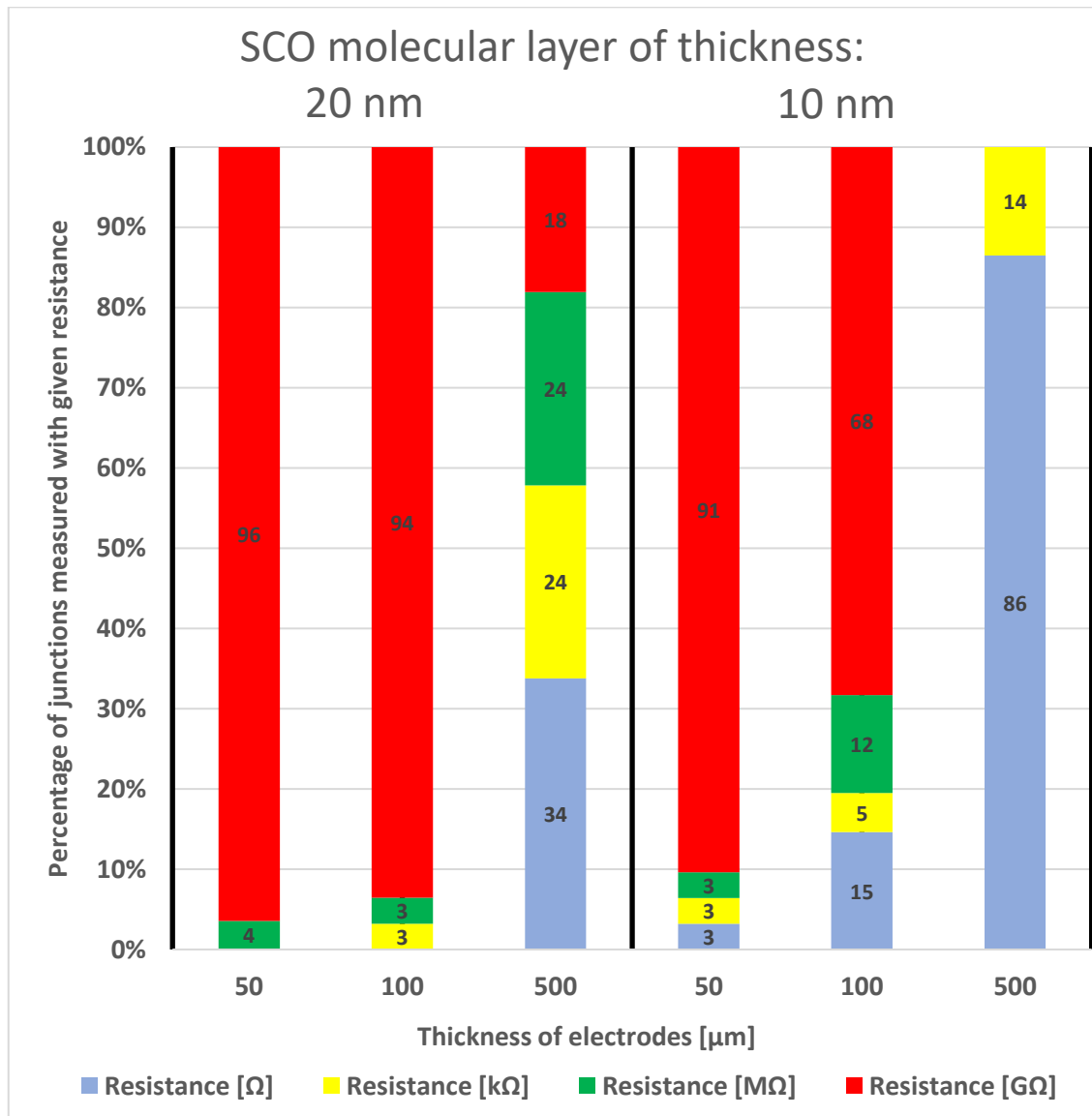

Figure 30: Graphical representation of statistic measurements of devices without carbon layer.

In the case of 60 nm SCO molecular layer devices are too insulating (with resistance predominantly in GΩ) for 50 μm and 100 μm thick. For 500 μm thick electrodes less resistive (MΩ and kΩ) junctions start to occur and some short circuits too (Ω range),

which is related to higher probability of short-circuits formation in the case of wider electrodes since the area where short-circuit can be formed is larger.

The 20 nm SCO molecular layer devices have still almost the same electric characteristics as previous ones, only 500 µm thick electrodes became even more short-circuited.

With the additional decrease of the thickness of the SCO molecular layer to 5 nm, we measured only short-circuited junctions, which can mean two things. Ether, the penetration of carbon atoms into the molecular layer is more than 5 nm, or Co atoms penetrate through both, 10 nm thick carbon layer and 5 nm thick molecular layer with a total penetration depth of more than 15 nm.

For this reason, we prepared next sample with 10 nm thick molecular layer. In this sample resistance reaches values in MΩ (43 %) and GΩ (32 %) for 50 µm. For 100 µm thick electrodes, insulating junctions were still the most frequent ones, nevertheless 22.2 % was in MΩ range. 500 µm thick electrodes are in this case already short-circuited.

According to this data, we can estimate, that the ideal thickness of SCO molecular spacing layer is around 10 nm for 50 µm and 100 µm thick electrodes. A bit thicker spacing layer between 20 nm and 60 nm suits better for 500 µm thick electrodes.

To compare results with those obtained for the samples without carbon layer by my colleague, it appears that carbon does not play any significant role in sense of short-circuits prevention.

Nevertheless, we have validated fabrication technique itself which means that we can use it for integration of varied kinds of other molecules since now. Next step will be to measure prepared devices in the cryostat to see if effect of SCO is visible in our spin-valves.

3 Conclusion and Perspectives

Within this master thesis, methods to integrate 2D materials and functional molecules/NPs into devices for molecular electronics and spintronics were investigated:

1. MoS_2-based horizontal transistor functionalized with SCO NPs was fabricated to investigate the impact of NPs SCO transition on MoS_2 electrical properties. Preliminary results indicate change of current through MoS_2 channel induced by SCO transition. The reason could be strain-induced change of band structure.

   Future work will focus on confirmation of obtained preliminary results by further measurements and testing of other SCO NPs (different size and/or different composition).

2. Method of MoS_2 integration into MTJ using transfer process to place the MoS_2 flake over the hole in the membrane to subsequently evaporate FM electrodes and in this way prevent their oxidation was investigated. Device was prepared without breaking the membrane, however, prepared sample resulted insulating, probably due to polymer residues which remained on the 2D material after the transfer process. The transfer process itself turned out to be difficult to perform since chance to lose 2D material and/or break the membrane is relatively high.

   Future work will focus on solving these problems. Annealing step before evaporation of FM electrodes could be the solution if the problem consists in polymer residues remaining on flake. Optimization of the transfer process will be also needed to make the technique more effective. In a far future, more exotic 2D materials, heterostructures of different 2D materials combined, and functional molecules/2D materials interfaces will be integrated.

3. Method of SCO molecules integration into vertical spin-valves as a thin spacer layer through their evaporation in UHV chamber was investigated. FM electrodes were prepared in cross-junction geometry using a set of shadow masks and carbon as a protective barrier. Non-short-circuited devices with thin SCO molecular spacer layer of 10 nm were prepared. Carbon did not show any significant effect on the prevention of short-circuits.

Future work will focus on measurement of these spin-valves in the cryostat. Other materials will also be considered and tested as a molecular spacer layer.

All these methods seem promising concepts towards the fabrication of more complex switchable devices for molecular electronics and spintronics to offer novel systems with new characteristics and new functionalities, which could be once yield in the semiconducting industry.

References

1. Moore, G. E. Cramming More Components Onto Integrated Circuits. *Proc. IEEE* **86**, 82–85 (1998).

2. Mack, C. A. Fifty Years of Moore's Law. *IEEE Trans. Semicond. Manuf.* **24**, 202–207 (2011).

3. Frank, D. J., Dennard, R. H., Nowak, E., Solomon, P. M. & and, Y. T. Device scaling limits of Si MOSFETs and their application dependencies. *Proc. IEEE* **89**, 259–288 (2001).

4. Geim, A. K. & Grigorieva, I. V. Van der Waals heterostructures. *Nature* **499**, 419–425 (2013).

5. Gobbi, M., Orgiu, E. & Samorì, P. When 2D Materials Meet Molecules: Opportunities and Challenges of Hybrid Organic/Inorganic van der Waals Heterostructures. *Adv. Mater.* **30**, 1706103 (2018).

6. Forment-Aliaga, A. & Coronado, E. Hybrid Interfaces in Molecular Spintronics. *Chem. Rec.* **18**, 737–748 (2018).

7. Rotjanapittayakul, W., Pijitrojana, W., Archer, T., Sanvito, S. & Prasongkit, J. Spin injection and magnetoresistance in MoS_2-based tunnel junctions using Fe_3Si Heusler alloy electrodes. *Sci. Rep.* **8**, (2018).

8. Dolui, K., Narayan, A., Rungger, I. & Sanvito, S. Efficient spin injection and giant magnetoresistance in Fe / MoS_2 / Fe junctions. *Phys. Rev. B* **90**, (2014).

9. Novoselov, K. S. *et al.* Electric Field Effect in Atomically Thin Carbon Films. *Science* **306**, 666–669 (2004).

10. Aliofkhazraei, M. *et al. Graphene Science Handbook: Mechanical and Chemical Properties*. (CRC Press, Taylor & Francis Group, 2016).

11. Aliofkhazraei, M. *et al. Graphene Science Handbook: Electrical and Optical Properties*. (CRC Press, Taylor & Francis Group, 2016).

12. Aliofkhazraei, M. *et al. Graphene Science Handbook: Applications and Industrialization*. (CRC Press, Taylor & Francis Group, 2016).

13. Duong, D. L., Yun, S. J. & Lee, Y. H. van der Waals Layered Materials: Opportunities and Challenges. *ACS Nano* **11**, 11803–11830 (2017).

14. Gupta, A., Sakthivel, T. & Seal, S. Recent development in 2D materials beyond graphene. *Prog. Mater. Sci.* **73**, 44–126 (2015).

15. Choi, W. *et al.* Recent development of two-dimensional transition metal dichalcogenides and their applications. *Mater. Today* **20**, 116–130 (2017).

16. Molybdenum Disulfide: Theory & Applications. *Ossila* Available at: https://www.ossila.com/pages/molybdenum-disulfide-mos2. (Accessed: 20th April 2019)

17. Li, X. & Zhu, H. Two-dimensional MoS_2: Properties, preparation, and applications. *J. Materiomics* **1**, 33–44 (2015).

18. Wang, Q. H., Kalantar-Zadeh, K., Kis, A., Coleman, J. N. & Strano, M. S. Electronics and optoelectronics of two-dimensional transition metal dichalcogenides. *Nat. Nanotechnol.* **7**, 699–712 (2012).

19. Peng, Q. & De, S. Outstanding mechanical properties of monolayer MoS_2 and its application in elastic energy storage. *Phys. Chem. Chem. Phys.* **15**, 19427–19437 (2013).

20. Wu, W. *et al.* Piezoelectricity of single-atomic-layer MoS_2 for energy conversion and piezotronics. *Nature* **514**, 470–474 (2014).

21. Splendiani, A. *et al.* Emerging Photoluminescence in Monolayer MoS_2. *Nano Lett.* **10**, 1271–1275 (2010).

22. Tong, X., Ashalley, E., Lin, F., Li, H. & Wang, Z. M. Advances in MoS_2-Based Field Effect Transistors (FETs). *Nano-Micro Lett.* **7**, 203–218 (2015).

23. Castellanos-Gomez, A. *et al.* Single-Layer MoS_2 Mechanical Resonators. *Adv. Mater.* **25**, 6719–6723 (2013).

24. Radisavljevic, B., Whitwick, M. B. & Kis, A. Small-signal amplifier based on single-layer MoS_2. *Appl. Phys. Lett.* **101**, 043103 (2012).

25. Yan, L., Shi, H., Sui, X., Deng, Z. & Gao, L. MoS_2-DNA and MoS_2 based sensors. *RSC Adv.* **7**, 23573–23582 (2017).

26. Lopez-Sanchez, O., Lembke, D., Kayci, M., Radenovic, A. & Kis, A. Ultrasensitive photodetectors based on monolayer MoS_2. *Nat. Nanotechnol.* **8**, 497–501 (2013).

27. Tsai, M.-L. *et al.* Monolayer MoS_2 Heterojunction Solar Cells. *ACS Nano* **8**, 8317–8322 (2014).

28. Zhu, J. *et al.* Boundary activated hydrogen evolution reaction on monolayer MoS_2. *Nat. Commun.* **10**, 1348 (2019).

29. Stephenson, T., Li, Z., Olsen, B. & Mitlin, D. Lithium ion battery applications of molybdenum disulfide (MoS2) nanocomposites. *Energy Environ. Sci.* **7**, 209–231 (2013).

30. Yue, Q. *et al.* Mechanical and electronic properties of monolayer MoS_2 under elastic strain. *Phys. Lett. A* **376**, 1166–1170 (2012).

31. Peña-Álvarez, M. *et al.* Single Layer Molybdenum Disulfide under Direct Out-of-Plane Compression: Low-Stress Band-Gap Engineering. *Nano Lett.* **15**, 3139–3146 (2015).

32. Scalise, E., Houssa, M., Pourtois, G., Afanas'ev, V. & Stesmans, A. Strain-induced semiconductor to metal transition in the two-dimensional honeycomb structure of MoS_2. *Nano Res.* **5**, 43–48 (2012).

33. Giménez Marqués, M. Stimuli-responsive magnetic coordination polymers: from crystals to nanoparticles. (2018).

34. Chaurasiya, R. S. & Hebbar, H. U. Reverse Micelles for Nanoparticle Synthesis and Biomolecule Separation. *Nanoscience in Food and Agriculture 4* 181–211 (Springer, Cham, 2017). doi:10.1007/978-3-319-53112-0_5

35. Galán-Mascarós, J. R. *et al.* Tuning Size and Thermal Hysteresis in Bistable Spin Crossover Nanoparticles. *Inorg. Chem.* **49**, 5706–5714 (2010).

36. Gudyma, I. V. & Ivashko, V. V. Spin-Crossover Molecular Solids Beyond Rigid Crystal Approximation. *Nanoscale Res. Lett.* **11**, (2016).

37. Collet, E. & Guionneau, P. Structural analysis of spin-crossover materials: From molecules to materials. *Comptes Rendus Chim.* (2018). doi:10.1016/j.crci.2018.02.003

38. Giménez-Marqués, M., Larrea, M. L. G.-S. de & Coronado, E. Unravelling the chemical design of spin-crossover nanoparticles based on iron(II)–triazole coordination polymers: towards a control of the spin transition. *J. Mater. Chem. C* **3**, 7946–7953 (2015).

39. Park, W. *et al.* Oxygen environmental and passivation effects on molybdenum disulfide field effect transistors. *Nanotechnology* **24**, 095202 (2013).

40. Dugay, J. *et al.* Phase Transitions in Spin-Crossover Thin Films Probed by Graphene Transport Measurements. *Nano Lett.* **17**, 186–193 (2017).

41. Giannazzo, F., Greco, G., Roccaforte, F. & Sonde, S. Vertical Transistors Based on 2D Materials: Status and Prospects. *Crystals* **8**, 70 (2018).

42. Felser, C., Fecher, G. H. & Balke, B. Spintronics: A Challenge for Materials Science and Solid-State Chemistry. *Angew. Chem. Int. Ed.* **46**, 668–699 (2007).

43. Bhatti, S. *et al.* Spintronics based random access memory: a review. *Mater. Today* **20**, 530–548 (2017).

44. Galbiati, M. Introduction to Spintronics. in *Molecular Spintronics* 3–17 (Springer, Cham, 2016). doi:10.1007/978-3-319-22611-8_1

45. Piquemal-Banci, M. *et al.* 2D-MTJs: introducing 2D materials in magnetic tunnel junctions. *J. Phys. Appl. Phys.* **50**, 203002 (2017).

46. Wu, H.-C. *et al.* Spin-dependent transport properties of $Fe_3O_4/MoS_2/F_3O_4$ junctions. *Sci. Rep.* **5**, 15984 (2015).

47. Morteza Najarian, A., Szeto, B., Tefashe, U. M. & McCreery, R. L. Robust All-Carbon Molecular Junctions on Flexible or Semi-Transparent Substrates Using "Process-Friendly" Fabrication. *ACS Nano* **10**, 8918–8928 (2016).

48. Rahman, S. F. A., Hashim, A. M. & Kasai, S. Graphene layer number determination from red-, green-, and blue-channel of optical images. in *2012 International Conference on Enabling Science and Nanotechnology* 1–2 (2012). doi:10.1109/ESciNano.2012.6149702

49. Li, H. *et al.* Rapid and Reliable Thickness Identification of Two-Dimensional Nanosheets Using Optical Microscopy. *ACS Nano* **7**, 10344–10353 (2013).

50. Coronado, E., Galán-Mascarós, J. R., Monrabal-Capilla, M., García-Martínez, J. & Pardo-Ibáñez, P. Bistable Spin-Crossover Nanoparticles Showing Magnetic Thermal Hysteresis near Room Temperature. *Adv. Mater.* **19**, 1359–1361 (2007).

51. Yang, Q., Fang, J., Zhang, G. & Wang, Q. Effect of substrate and temperature on the electronic properties of monolayer molybdenum disulfide field-effect transistors. *Phys. Lett. A* **382**, 697–703 (2018).